Estimating stomatal conductance and evapotranspiration of winter wheat using a soil-plant water relations-based stress index

Xun Wu[a], Yanqi Xu[b], Jianchu Shi[b], Qiang Zuo[b*], Ting Zhang[b], Lichun Wang[c], Xuzhang Xue[c], Alon Ben-Gal[d]

[a] College of Water Resources and Civil Engineering, China Agricultural University, Beijing 100083, China

[b] College of Land Science and Technology, China Agricultural University; Key Laboratory of Plant-Soil Interactions, Ministry of Education; and Key Laboratory of Arable Land Conservation (North China), Ministry of Agriculture, Beijing 100193, China

[c] National Research Center of Intelligent Equipment for Agriculture, Beijing 100097, China

[d] Soil, Water and Environmental Sciences, Agricultural Research Organization, Gilat Research Center, mobile post Negev 85280, Israel

[*] Corresponding authors.

Tel.: + 86 10 62732504; Fax: + 86 10 62733596.

E-mail address: qiangzuo@cau.edu.cn (Q. Zuo).

E-mail addresses for the other coauthors:

wuxun232425@163.com (X. Wu)

yq_Xu1995@163.com

shijianchu@cau.edu.cn (J. Shi)

tzztsn@163.com (T. Zhang)

wanglc@nercita.org.cn (L. Wang)

xuexz@nercita.org.cn (X. Xue)

bengal@volcani.agri.gov.il (A. Ben-Gal)

Abstract

Stomatal conductance, closely related to water flow in the soil-plant-atmosphere continuum, is an important parameter in the Penman-Monteith (P-M) model for estimating evapotranspiration (ET). In this study, a novel soil water stress index ω, considering intrinsic soil-plant water relations, was introduced into the Jarvis empirical estimation model of stomatal conductance to improve the representation of the effect of soil water stress on stomatal conductance. The index ω accounted not only for current water availability by combing the effects of relative distribution of soil water to roots and nonlinear stomatal response, but also for the hysteresis effect of water stress by means of the inclusion of a recovery coefficient. Combined plant and soil-based measurements from a greenhouse experiment provided the basis for investigating the relationship between leaf stomatal conductance g_s and root zone soil water stress represented by ω. The response of g_s to root-weighted soil matric potential was found to be nonlinear. The relationship between g_s and the extent of previous water stress (i.e. the water stress recovery coefficient curve) was generalized by a power function and was verified and confirmed using results obtained from the literature. The reliability of ω was tested by coupling it into the Jarvis model to estimate leaf (g_s) and canopy (g_c) stomatal conductance, and thereupon into the P-M model to estimate cumulative ET (CET) in the greenhouse experiment and two field experiments. The estimated g_s, g_c and CET agreed well with the measurements, with root mean squared error not more than 0.0006 m s^{-1}, 0.0020 m s^{-1} and 8.2 mm, respectively, and determination coefficient (Nash-Sutcliffe efficiency coefficient) consistently greater than 65%

(0.14). Therefore, ω should be feasible and reliable to delineate the response of stomatal physiological reaction to water stress, and hence helpful for accurate estimation of ET using Jarvis-based P-M models.

Key words:

Water stress; Soil-plant water relations; Penman-Monteith; Soil matric potential; Jarvis model

1. Introduction

Through direct control of gas and energy exchanges between plants and the atmosphere, stomata affect plant growth, ecosystem function, and atmospheric composition (Misson et al., 2004; Ono et al., 2013). As a measure of the magnitude of stomatal aperture, stomatal conductance plays a critical role in driving both water flow and solute transport in the soil-plant-atmosphere continuum (SPAC) (Damour et al., 2010; Bai et al., 2017), and thus is considered a key and complex variable in hydrological modeling for the estimation of plant water use in the earth's critical zone. To represent individual and group stomatal behavior, stomatal conductance is usually divided into leaf (g_s) and canopy (g_c) components. In the widely used Penman-Monteith (P-M) evapotranspiration (ET) model (Monteith, 1965), g_c is the sole parameter reflecting plant water physiological regulation or adaptation. Accurate quantification of stomatal conductance is very important for understanding plant stomatal behavior and evaluating reliable ET, particularly when using the P-M model.

Limited by tremendous difficulty in practical measurements, stomatal conductance is often simulated using both mechanistic and empirical models (Damour et al., 2010). Such models are based on a plant's internal stomatal response mechanisms to physiological processes, and on experimentally determined correlations between stomatal conductance and various environmental factors. Almost all the mechanistic models, which are usually comprehensive and complicated, require a set of water-related physiological parameters (such as guard cell osmotic pressure and xylem hydraulic conductivity) that are difficult to obtain (Egea et al., 2011). The empirical models are therefore more popularly and readily employed due to their simplicity. Up until now, a large number of empirical models have been proposed. The archetypal Jarvis model (Jarvis, 1976; Stewart, 1988) simply assumes g_c as a product of effective leaf area index and g_s

estimated using a multiplicative algorithm that decreasingly adjusts the reference or maximum value of leaf stomatal conductance according to environmental factors such as solar radiation, air temperature, water vapor pressure deficit, CO_2 concentration, and drought stress.

Drought stress causes widespread detrimental effects on crop water use, growth and productivity, especially in arid and semi-arid regions and therefore, much attention has been paid to the relationship between it and g_s. In the original or modified Jarvis models, two alternative approaches have been utilized to account for stomatal response to drought stress. One is based on plant water potential (e.g. leaf/stem water potential), a sensitive indicator for plant water status (Jarvis, 1976; Nortes et al., 2005). The second approach is based on root zone soil water and its availability for uptake by plants. The soil-based approach appears more feasible due to relative ease in observing and quantifying soil water dynamics compared to leaf/stem water potential dynamics, especially under field conditions. Soil water stress response is often described as a linear function of the averaged root-zone soil water content/matric potential (Mahfouf et al., 1996; Sellers et al., 1996; Porporato et al., 2001; Arora, 2003; Keenan et al., 2010; Li et al., 2013). As a consequence of oversimplifying soil-plant water relations, such soil water-based approaches, although widely adopted to estimate g_s using different Jarvis-type models, are prone to three oversights or omissions as follows. Firstly, averaged root-zone soil water content/matric potential is not sufficient to describe the availability of soil water to plants. Besides soil water content, the relative distribution of soil water to roots was also found to significantly impact its availability to root water uptake (Šimůnek and Hopmans, 2009; Shi et al., 2015). Obviously, the more consistent the distributions between soil water and roots are (i.e. more water is located in the zone with more roots), the stronger the transpiration by stomata, and correspondingly, the higher the stomatal conductance may be. Ignoring the relative distribution of soil water to roots likely leads to uncertain and incorrect evaluation of the degree that plants are exposed to water stress, especially for situations with uneven distributions of soil water and/or roots. Secondly, assuming a linear function for stomatal response to soil water deficit is inaccurate. A nonlinear function, including at least one fitting parameter, appears to be superior in accurately describing the effect of soil water deficit on stomatal aperture (Egea et al., 2011; Wang et al., 2014). This is because the reduction of g_s is dependent not only on the magnitude of soil water deficit but also on various eco-physiological regulation mechanisms, such as plant resistance/tolerance/avoidance to drought (Guswa et al., 2004). The flexibility or adjustability of a nonlinear response function in shape, represented by the fitting parameters, would implicitly account for such plant self-regulation mechanisms, at least to some extent (Wu et al., 2020a). Lastly, the hysteresis effect of soil water stress on g_s is not considered in the Jarvis-type models. The stomatal conductance of a previously stressed plant is often observed to recover or rise gradually after re-watering even when soil water deficit is thoroughly relieved rapidly (Souza et al., 2004; Galmés et al., 2007; Virlouvet and Fromm, 2015). Following stress, the time necessary for g_s to return to its potential level may be delayed for several days or even more (Dörffling et al., 1977; Pou et al., 2008). In conventional ecological and hydrological models, plant physiological recovery from drought is often assumed to be complete and relatively fast, synchronizing with the fluctuation in current soil water availability, which is at odds with the current understanding of physiological mechanisms in many ecosystems (Ogle et al., 2015). Thus, ignoring the offsets between plant and soil water status (i.e. the hysteresis of water stress) might result in erroneous estimation of g_s and ET using Jarvis-type models.

Recent advancements may provide possible solutions for the three aforementioned oversights. Soil water availability to plants was evaluated using a root-weighted method by combining the effects of amount of root-zone soil water and its relative distribution to roots, with the normalized root length density as a weighting factor for soil water (Shi et al., 2015; Wu et al., 2017). As an alternative of linear expression, a nonlinear function can more readily describe the dynamics of stomatal response to soil water deficit (Rallo and Provenzano, 2013; Wu et al., 2020a). A soil water stress index ω, originating from the root-water-uptake model proposed by Feddes et al. (1976), was put forward to improve the original soil water stress response function by introducing a water stress recovery coefficient δ to consider the hysteresis effect of water stress on root water uptake (Wu et al., 2020b). The recovery coefficient δ was found to viably represent the hysteresis characteristics of root water uptake, and to be applicable for estimating transpiration and simulating soil water flow during drought and re-watering cycles in a soil-wheat system. Undoubtedly, the applicability of a recovery coefficient δ, proposed based on measurements and modeling of root water uptake and transpiration, must be verified for characterizing the hysteresis effect of soil water stress on stomatal behavior. In addition, the accuracy and reliability of estimating stomatal conductance from the Jarvis model, and thereupon determining ET using the P-M model, requires verification.

The objectives of this study were to (1) investigate and quantify the effects of root zone soil water status (e.g. the current and previous water availability) on stomatal conductance; and (2) introduce a novel soil water stress index ω to characterize the effect of drought stress and to improve the estimation accuracy and reliability of stomatal conductance by the Jarvis model and ET by the P-M model. The relationship between g_s and root-zone soil water status, and the quantitative description of the hysteresis effect of antecedent water stress on g_s by incorporating a water stress recovery coefficient δ, were explored using data from a greenhouse experiment. The quantification of δ was further verified via a large amount of stomatal conductance data retrieved from literature. The accuracy and reliability of the index ω was tested by coupling it into the Jarvis model to estimate leaf (g_s) and canopy (g_c) stomatal conductance, and thereupon into the P-M model to estimate cumulative ET (CET) for cases of the greenhouse experiment and two additional field experiments.

2. Materials and methods

2.1 Greenhouse soil column experiment (Exp. 1)

2.1.1 Experimental conditions and treatments

A soil column experiment on winter wheat (*Triticum aestivum* L. *Nongda* 212) in a greenhouse at the Key Laboratory of Plant-Soil Interactions (MoE, Ministry of Education) in China Agricultural University, Beijing, China, described in detail by Wu et al. (2020b), was employed to investigate the relationship between leaf stomatal conductance g_s and root-zone soil water status. 288 polyvinyl chloride (PVC) columns (15 cm in diameter, 55 cm in depth) were manually assembled for cultivating winter wheat. Each column was packed with 2 cm thick fine quartz sand at the bottom and then covered by a piece of filter paper, on which air-dried clay loam soil was filled up to the height of 50 cm at a bulk density of 1.38 g cm^{-3}. Soil texture and hydraulic properties of the homogeneous media are shown in Table 1. On 11 October 2015, three seeds after germination were sown in each soil column. To minimize soil surface evaporation, all columns were mulched with 3 cm thick fine quartz sand at soil surface on 20 days after sowing (DAS). During the experimental period, ambient conditions were kept as: photosynthetic photon flux density of 500 μmol m^{-2} s^{-1} at the plant height for 12 h d^{-1} (from 06:00 to 18:00); day/night air temperature of 30/12 ± 2 °C; relative humidity of 40 ± 5%.

All columns were uniformly irrigated to field capacity daily before 27 DAS, and consequently irrigation was scheduled according to the plant water deficit index (PWDI) calculated from root-weighted soil matric potential (Wu et al., 2017). The PWDI, ranging between 0 and 1, was used to represent the degree that plants were exposed to water stress, with higher PWDI value indicating more severe water stress. During the water treatment periods (28-110 DAS), five treatments (W1, W2, W3, W4 and W5) were applied by triggering irrigation using different pre-designed thresholds of PWDI. For full irrigation treatment W1, the PWDI threshold was fixed as 0.02 during all treatment periods. For the other four water stress treatments, W2-W5, the PWDI thresholds were designed on the basis of two divided periods, specified as 0.05, 0.07, 0.15, 0.30 in the first period (28-60 DAS), and 0.07, 0.13, 0.30, 0.55 in the second period (61-110 DAS), to analyze the effects of various degrees of previous water stress on plant water use (Wu et al., 2020b). The supplied water amount for each irrigation event was calculated according to the difference between the measured root-zone soil water content and field capacity (target water content).

2.1.2 Measurements

Soil moisture content in three soil columns chosen from each treatment was measured by previously calibrated time domain reflectometry probes (TDR 100, Campbell, USA) at the depths of 5, 10, 15, 25, 35 and 45 cm, from which the corresponding soil matric potential was determined using soil water retention characteristics (Table 1). Samplings were conducted in three entire irrigation cycles (between two successive irrigation events) at mid-tillering, jointing and heading stages of winter wheat, corresponding to 42-49, 71-78 and 103-110 DAS, respectively. There were small differences in the actual days of sampling between treatments due to different PWDI thresholds to trigger irrigation and consequential different dates of irrigation events. During each sampling (i.e. irrigation or watering-drying) period, three replicate columns were randomly selected from each treatment daily to measure stomatal conductance of the youngest fully expanded leaves from 8:00 to 11:00 with a portable photosynthesis measurement apparatus (Li-6400, Li-Cor, USA). The selected columns were cut open following shoot removal to sample soil and roots from the surface to maximum rooting depth at 5 cm intervals. A portion of each soil sample was oven-dried to determine soil water content for TDR validation. The remainder of each soil layer was washed and sieved on a 0.5 mm diameter screen to collect roots. Roots were scanned and analyzed with the WinRHIZO software package (Regent Instruments Inc., Canada) to obtain root length.

2.2 Field lysimetric experiment (Exp. 2)

2.2.1 Experimental conditions and treatments

A field lysimetric experiment, also introduced in detail in Wu et al. (2020b), was conducted from September 2014 to June 2015 at the National Experimental Station for Precision Agriculture (40°10′31″ N, 116°26′10″ E, altitude 50.1 m) in Changping District, Beijing, China, to evaluate ω in the Jarvis model. Winter wheat seeds (same cultivar as Exp. 1) were sown in 10 weighing lysimeters (230 cm high × 75 cm wide × 100 cm long, 0.05 mm in precision) at a density of 6.7×10^6 plants ha^{-1} on 29 September 2014. The steel box of each lysimeter was filled in by excavating original soil monoliths taken from a nearby field, with three undisturbed distinct loam layers (Table 1).

Until heading stage of winter wheat (203 DAS), all lysimeters were uniformly managed with 51.0 mm overwintering water. Subsequently, five water treatments (WT0, WT1, WT2, WT3 and WT4) were applied with two replicates as a result of limited number of lysimeters available. For treatment WT0, irrigation was supplied every 3 days. For treatments WT1-WT4, irrigation was scheduled empirically according to the local practice. More specifically, treatment WT1 was irrigated 45, 51 and 63 mm at booting, flowering and maturing stages (215, 229 and 238 DAS), respectively; WT2 35 and 59 mm at flowering and maturing stages (224 and 238 DAS); WT3 66 mm at jointing stage (194 DAS); For WT4 there was no irrigation during the water treatment periods. A movable rain-shelter was utilized to prevent precipitation reaching the lysimeters from turning-green until harvest.

2.2.2 Measurements

From heading to maturing stage (203-244 DAS), soil water content in each lysimeter was measured daily by a calibrated capacitance probe (Diviner 2000, Sentek, Australia) at 10 cm intervals from soil surface to 160 cm depth, and used to obtain the soil matric potential as described in Exp. 1. Four representative plants were randomly chosen from the full irrigation treatment WT0 to measure stomatal conductance of the youngest fully expanded leaves at 9:30-11:30 every 1 d to 3 d as described in Exp. 1, in order to obtain the maximum g_s of winter wheat (g_{smax}) in the field. Daily ET was determined according to the change of the lysimeter weight recorded by the automatic weighing system. Five plants from each lysimeter were pre-selected to measure the length and width of green leaves and plant height every 5 d to 7 d. Leaf area was estimated as a product of the measured length, width and a measured conversion coefficient of 0.77 (Wu et al., 2017). Conventional meteorological data such as air temperature, relative humidity, solar radiation, wind velocity and precipitation were automatically recorded at 30 min intervals by an agro-meteorological station (WeatherHawk 500, Campbell Scientific, USA). The dynamics of main meteorological variables from jointing until mature (197-243 DAS) are shown in Fig. 1a.

2.3 Field drip irrigation experiment (Exp. 3)

2.3.1 Experimental conditions and treatments

From October 2019 to June 2020, a drip irrigation experiment for winter wheat (*Triticum* *aestivum* L. *Jinan* 17) was conducted at the Modern Agriculture Experimental Demonstration Base in Yellow River Delta (37°19′17″ N, 118°38′41″ E, altitude 14.0 m), located in Dongying City, Shandong Province, China, in order to further validate the accuracy and reliability of the index ω. The Yellow River Delta, lying on the south side of Bohai Sea, is characterized by a temperate, semi-humid continental monsoon climate, with annual mean precipitation of around 590 mm, most of which falls between June and September. Affected by shallow saline groundwater, the entire delta is covered mainly by varying degrees of saline soils (Xu et al., 2004). The groundwater table was maintained at around 112 cm below the surface during the experiment (from April to June 2020), and the averaged root-zone salt content was observed to be as low as around 1.87 g kg^{-1}, likely as a result of leaching due to a series of heavy rainfall events prior to the experiment including Super Typhoon Lekima in August 2019. The soil profile in the experimental field comprises three distinct loam layers, whose physical properties are also shown in Table 1.

On 3 October 2019, winter wheat seeds were sowed in 12 plots (900 cm long × 600 cm wide) at a plant density of 6.7×10^6 plants ha^{-1} and a narrow-wide row spacing (with 10 cm in narrow row spacing, 50 cm wide, and 1 cm for plant spacing, Fig. 2). One drip tape, with emitter interval of 30 cm and discharge rate of 2.34 L h^{-1}, were set at the center of eight adjacent narrow rows (Fig. 2). From sowing to 18 April 2019 (198 DAS), winter wheat in each plot was irrigated uniformly with 50 mm water (22 mm for germination and 28 mm for jointing) supplementing 85.6 mm precipitation. Subsequently, four irrigation treatments (T1, T2, T3 and T4) were applied with 3 replicates. Under treatments T1-T3, irrigation was scheduled using the PWDI estimated based on root-weighted soil matric potential (Wu et al., 2017), with PWDI thresholds of 0.1, 0.2 and 0.4, respectively, used to trigger irrigation. Field capacity was taken as the target water content. Treatment T4 was exclusively rain-fed without any irrigation. Meteorological data including rainfall during the experiment is shown in Fig. 1b. Calcium superphosphate (90 kg hm^{-2}) and potassium oxide (90 kg hm^{-2}) were supplied as basal fertilizers before sowing. Urea dissolved in a steel fertilizer tank was supplied simultaneously along with irrigation water. The total urea supply was 135, 77 and 22 kg hm^{-2} for T1-T3, respectively, and no urea was supplied for rain-fed treatment T4.

2.3.2 Measurements

The calibrated time domain transmission probes (SDI12, Swstek, Canada) were used to measure soil water content and electrical conductivity daily at depths of 5, 10, 20, 30, 50, 70 and 90 cm in one replicate plot selected from each treatment. At the jointing, booting, flowering, filling and maturing stages (197, 205, 214, 225 and 235 DAS), three plants from each treatment were randomly selected to measure the length and width of green leaves, and plant height. Leaf area was obtained as described in Exp. 2. Meteorological data (Fig. 1b) were monitored automatically by the same type agro-meteorological station as that in Exp. 2.

2.3.3 Water balance analysis

During a designed balance period for a specific treatment plot in Exp. 3, the cumulative ET (CET, mm) was calculated using the following water mass balance equation:

$$\mathrm{CET} = I + P - R - Q - \Delta W \tag{1}$$

where I is irrigation (mm); P is precipitation (mm); R is surface runoff (mm), which was not observed during the entire experimental period and thus ignored; Q is water flux across the lower boundary (mm), calculated according to Darcy's law (Hasegawa and Eguchi, 2002); ΔW (mm) is the change of water stored in the soil profile from surface to the lower boundary, which was fixed as 90 cm and larger than the measured maximum rooting depth of local winter wheat.

2.4 Penman-Monteith model to estimate evapotranspiration

An energy balance based Penman-Monteith (P-M) model was employed to estimate ET as (Monteith, 1965):

$$\lambda \mathrm{ET} = \frac{\Delta(R_n - G) + \rho_a C_p\, D/r_a}{\Delta + \gamma\left[1 + 1/(g_c r_a)\right]} \tag{2}$$

where λ is the latent heat of vaporization (MJ kg^{-1}); ET is crop daily evapotranspiration (mm d^{-1}); Δ is the slope of water vapor saturation pressure versus temperature curve (kPa K^{-1}); R_n is net radiation (W m^{-2}); G is soil heat flux (W m^{-2}); C_p is specific heat of dry air at constant pressure (MJ kg^{-1} K^{-1}); ρ_a is air density (kg m^{-3}); D is water vapor pressure deficit (kPa); γ is psychrometric constant (kPa K^{-1}); g_c is canopy stomatal conductance (m s^{-1}); r_a is aerodynamic resistance (s m^{-1}), calculated as (Thom, 1972):

$$r_a = \frac{\ln\left((Z\text{-}d)/(H_c - d)\right)\ln\left((Z\text{-}d)/Z_0\right)}{k^2 u} \tag{3}$$

where Z is reference height (m); H_c is crop height (m); k = 0.41, is Karman constant; u is wind speed at the reference height (m s^{-1}); $d = 0.67H_c$, is zero plane displacement (m); $Z_0 = 0.13H_c$, is the roughness length of the crop relative to momentum transfer (m).

2.5 Jarvis model to estimate stomatal conductance

An empirical Jarvis model was utilized to estimate canopy stomatal conductance g_c in Eq. (2) as (Jarvis, 1976; Stewart, 1988):

$$g_c = g_s LAI_e \tag{4}$$

$$LAI_e = \frac{LAI}{0.3LAI + 1.2} \tag{5}$$

where LAI_e is the effective leaf area index (cm^2 cm^{-2}) (Ben-Mehrez et al., 1992); LAI is the leaf area index (cm^2 cm^{-2}). The leaf stomatal conductance g_s (m s^{-1}) was estimated as:

$$g_s = g_{s\max} f(R_s) f(T) f(D) f(h_{ave}) = g_{s0} f(h_{ave}) \tag{6}$$

in which,

$$f(R_s) = \frac{R_s(1000 + k_{Rs})}{1000(R_s + k_{Rs})} \tag{7}$$

$$f(T) = 1 - k_T(25 - T) \tag{8}$$

$$f(D) = 1 - k_D D \tag{9}$$

$$f(h_{ave}) = 1 - \frac{h_{ave} \text{-} h_C}{h_W \text{-} h_C} \tag{10}$$

where $g_{s\max}$ is species-dependent maximum g_s under optimal conditions (Li et al., 2019), determined as 0.012 m s^{-1} according to the measurements in the field; R_s is solar radiation (W m^{-2}); T is air temperature (℃); D is water vapor pressure deficit (kPa); g_{s0} is the g_s under optimal soil water condition (m s^{-1}); k_{Rs}, k_T and k_D are the weather dependent fitting parameters; h_{ave} is arithmetic average of soil matric potentials over the root zone (cm); $f(h_{ave})$ is soil water stress response function, quantifying the effect of soil water deficit; h_C and h_W are the thresholds of optimal soil water condition and wilting point (cm), adopted as the recommended values of -400 and -15000 cm, respectively (Feddes et al., 1976).

2.6 Soil water stress index ω

The soil water stress index ω (Wu et al., 2020b) was directly employed to the Jarvis model by replacing $f(h_{ave})$ in Eq. (6) as:

$$\omega = \delta \int_0^1 f(h) L_{nrd}(z_r)\, \mathrm{d}z_r \tag{11}$$

Combining Eqs. (6) and (11) yields:

$$g_s = g_{s0}\omega \tag{12}$$

where δ is the water stress recovery coefficient, used to characterize the hysteresis effect of water stress anteriorly suffered by plants; the integral $\int_0^1 f(h)L_{nrd}(z_r)dz_r$ (i.e. root-weighted response function) represents the current root-weighted soil water availability, in which h is soil matric potential (cm); z_r is normalized soil depth originating from the soil surface and positive downwards, i.e. the ratio of soil depth to the maximum rooting depth; $L_{nrd}(z_r)$ is normalized root length density (NRLD), obtained through fitting the measured data with a two-order polynomial equation as ($R^2 = 0.86$):

$$L_{nrd}\left(z_r\right) = 2.50z_r^{\,2} - 3.99z_r + 2.20 \tag{13}$$

in Exp. 1 (Wu et al., 2020a, b), and estimated using a generalized function in both Exp. 2 and Exp. 3 as (Zuo et al., 2013):

$$L_{nrd}\left(z_r\right) = p\left(1 - z_r\right)^{p-1} \tag{14}$$

where p is the NRLD at the soil surface, recommended as 3.85 for wheat.

A piecewise power function was selected for the response function $f(h)$ as (Musters and Bouten 1999):

$$f(h) = \begin{cases} 1 & h \geq h_C \\ 1 - \left(\dfrac{h\text{-}h_C}{h_W\text{-}h_C}\right)^{\rho} & h_W < h < h_C \\ 0 & h \leq h_W \end{cases} \tag{15}$$

where ρ is a fitting parameter: $\rho = 1$ defines a linear shape as the same as Eq. (10); the convex shape with $\rho > 1$ shows significantly sharp reduction of g_s only for extreme soil water deficit; vice versa, the concave shape with $0 < \rho < 1$ demonstrates rapid reduction of g_s even for slight soil water deficit. Compared with the linear response function of Eq. (10), Eq. (15) should be more flexible and adjustable in shape, and thus more feasible and reasonable to describe the effect of soil water deficit on stomatal conductance.

The water stress recovery coefficient δ in Eq. (11) was also described as a power function of the plant water deficit index (PWDI) on the previous day (Wu et al., 2020b), which was simplified from quantitatively investigating the integrated effects of historical water stress events and validated through Exp. 1, viz.:

$$\delta=(1\text{-PWDI}_{t-1})^{\mu} \tag{16}$$

where t is time (d); μ is fitting parameter. As for the hysteresis in transpiration, $\text{PWDI}_{t\text{-}1}$ = 1- $\omega_{t\text{-}1}$ = 1- $\text{RTR}_{t\text{-}1}$, in which $\text{PWDI}_{t\text{-}1}$ is the PWDI on the previous day to quantify the extent of early soil water stress, and RTR is the relative transpiration rate (Wu et al., 2020b). Hence for the stomatal conductance,

$$\text{PWDI}_{t\text{-}1}=1\text{-}\omega_{t\text{-}1}=1\text{-}\left(\frac{g_s}{g_{s0}}\right)_{t\text{-}1} \tag{17}$$

Similarly as for transpiration/root-water-uptake by Wu et al. (2020b), Eq. (16) was further verified by investigating the relationship between g_s and the extent of soil water stress previously suffered by winter wheat (i.e. $\text{PWDI}_{t\text{-}1}$ computed by Eq. (17)) in Exp.1. Besides the verification data from Exp. 1, to supplement the samples and thereby justify the feasibility and reliability of Eq. (16) for different plants under different environmental conditions, we searched a great deal of literature for data describing recovery processes of g_s after re-watering. The literature was retrieved from the following databases: ScienceDirect, Web of Science Series, Baidu Scholar, China National Knowledge Infrastructure (CNKI), and Chinainfo, using retrieval keywords "stomatal behavior/stomatal conductance/gas exchange" + "re-watering/recovery/after-effect" for the period between 1970 and 2019. From the retrieved literature in English and Chinese, we selected papers that documented the daily measured g_s of stressed and control plants after re-watering. The procedure resulted in 17 data sets, each with at least six sample points, originating from 15 papers (Fischer et al., 1970; Boussiba and Richmond, 1976; Sanchez et al., 1982; Torrecillas et al., 1995; Dry and Loveys, 1999; Liang and Zhang, 1999; Marron et al., 2002; Flexas et al., 2004; Miyashita et al., 2005; Galle et al., 2011; Pou et al., 2012; Jin et al., 2012; Perez-Martin et al., 2014; Liu et al., 2015; Iovieno et al., 2016). The data sets encompassed twelve plant species belonging to field crops (i.e. kidney beans, tomato, maize), herbs (tobacco), vines (grape), and trees (olive, rockrose, oak, leucaena, thuja, acacia and populus) under various greenhouse or natural environmental conditions including different soils (loam, sandy loam, clay soil, and mixed soil, etc.), water treatments (full and deficit water supply levels), nutrient supplies (N, P, K and other microelements), and other variables. Based on the retrieved data sets, the relationship between g_s and $\mathrm{PWDI}_{t\text{-}1}$ was analyzed for each of the twelve plants.

2.7 Parameter optimization and model performance evaluation

Five fitting parameters, k_{Rs}, k_T, k_D, ρ and μ, were optimized with the nonlinear least-squares method, provided in the Programming Solver of Microsoft Office Excel (Wraith and Or, 1988). The objective function (OF) to be minimized in the algorithm was set as:

$$\mathrm{OF}(\chi) = \sum_{i=1}^{n} \left[I_i^{obs} - I_i^{est}(\chi) \right]^2 \tag{18}$$

where χ is the vector of the optimized parameters; i = 1, 2, …, n is the serial number of measurements; I_i^{obs} and $I_i^{est}(\rho)$ are respectively the measured and estimated g_s (Exp. 1), g_c (Exp. 2) or CET (Exp. 3), dependent on the available data in various experiments.

Three statistical indices including the root mean squared error (RMSE), the coefficient of determination (R^2), and the Nash-Sutcliffe efficiency coefficient (NSE) were employed to evaluate the model performance:

$$\text{RMSE} = \sqrt{\frac{1}{n}\sum_{i=1}^{n}(O_i - S_i)^2} \tag{19}$$

$$R^2 = \frac{\left[\sum_{i=1}^{n}(O_i - \overline{O})(S_i - \overline{S})\right]^2}{\sum_{i=1}^{n}(O_i - \overline{O})^2 \cdot \sum_{i=1}^{n}(S_i - \overline{S})^2} \tag{20}$$

$$\text{NSE} = 1 - \frac{\sum_{i=1}^{n}(O_i - S_i)^2}{\sum_{i=1}^{n}(O_i - \overline{O})^2} \tag{21}$$

where O_i and S_i are the measured and estimated values, respectively; $\overline{O}$ and $\overline{S}$ are the mean measured and estimated values, respectively.

3. Results and discussion

3.1 Effect of soil water stress on leaf stomatal conductance

3.1.1 Relationship between leaf stomatal conductance and soil water status

In order to synthesize the effect of root distribution and root-zone soil water condition and obtain effective root zone hydraulic status sensed by the plant, the root-weighted soil matric potential (h_{RW}, cm) was calculated according to the generalized two-order polynomial NRLD function Eq. (13) and daily measured distributions of soil matric potential in Exp. 1 through (Cai et al., 2017; Wu et al., 2017):

$$h_{RW} = \int_0^1 h(z_r) L_{nrd}(z_r)\,\mathrm{d}\,z_r \tag{22}$$

in which, $\begin{cases} h(z_r) = h_C & \text{when } h(z_r) \geq h_C \\ h(z_r) = h_W & \text{when } h(z_r) \leq h_W \end{cases}$

During each irrigation period, h_{RW} under full irrigation treatment W1 changed between -730 and -460 cm with a mean of -570 cm, corresponding to soil water content (SWC) of 80% field capacity as designed. Under deficit irrigation treatments W2-W5 (Fig. 3a-3d), h_{RW} was significantly affected by irrigation and root water uptake, increased to the maximum (close to optimal soil water threshold h_C) immediately after irrigation, and decreased sharply following a slow attenuation of 2-4 days. Average h_{RW} on the day prior to irrigation under W2-W5 reached -2501, -3102, -5598 and -8128 cm, respectively, corresponding to SWCs of 50%, 48%, 42% and 40% field capacity, indicating that the winter wheat was subjected to increasing intensity of water stress as per design.

Fig. 3 also shows the actual daily g_s under W2-W5 in Exp. 1 and the corresponding potential g_s (i.e. g_{s0}, the g_s measured from W1) during different sampling (irrigation) periods. Slight fluctuation was observed for g_{s0} under treatment W1 due to the basically stable controlled indoor conditions and sufficient water supply, whereas actual g_s under deficit irrigation treatments W2-W5 changed greatly during each watering-drying cycle and was significantly suppressed prior to each irrigation when actual g_s declined from W1 to W5 as soil water stress intensified. Not like the fast recovering process of h_{RW} when the soil water deficit condition was immediately ameliorated by irrigation, g_s was found to recover gradually, reach its periodical peak 1-3 d slower than h_{RW}, and subsequently decrease from the peak until the end of a cycle. The lower the h_{RW} prior to irrigation, the more slowly and incompletely the plant (g_s) recovered. For example, g_s in W2 rose to the potential level (g_{s0}) about 2 days after irrigation, while under W5, the recovery duration was usually 3 days reaching only about 80% of g_{s0}. Similar recovery dynamics for g_s, essentially attributed to the hysteresis effect of water stress (Stalfelt, 1955; Bengtson et al., 1977), were also reported by many other researchers (Miyashita et al., 2005; Izanloo et al., 2008; Chen et al., 2010). Stomatal regulation in response to drought and its recovery process is complicated, involving a variety of chemical and hydraulic signals or mechanisms (Comstock, 2002; Tardieu et al., 2010). Some studies related the lowering down of g_s (or closure of stomata) to elevated abscisic acid content in the plant suffering from drought stress, while attributing the slow recovery of stomatal conductance (or re-opening of stomata) after re-watering to the loss or limitation of plant hydraulic conductivity caused by the previous water stress (Pou et al., 2008; Blackman et al., 2009; Chen et al., 2010). The relative stomatal conductance (g_s/g_{s0}) decreased with decreasing h_{RW}, demonstrating a more nonlinear pattern of changing process (Fig. 4), as reported by Egea et al. (2011) and Wang et al. (2014). The concave shape between g_s/g_{s0} and h_{RW} showed that g_s was sensitive to a wide range of available soil water conditions (represented by the root-weighted soil matric potential h_{RW} in Fig. 4). A sharp increase in g_s/g_{s0} (or g_s) would result from a slight increase of h_{RW} in the high root-weighted soil matric potential range of $h_{RW} >$ -3000 cm (i.e. with more available water for root uptake). In addition, the fitted curve of g_s/g_{s0} to h_{RW} by nonlinear function was found to be generally above the measured g_s/g_{s0} during recovery after rehydration, as shown in the insert in Fig. 4 (with h_{RW} higher than -500 cm), which might be attributed to the fact that the nonlinear response function only considered the current soil water availability but ignored the hysteresis of stomatal recovery from previous water stress (Shi et al., 2014).

3.1.2 Leaf stomatal conductance as a function of previous water stress

Fig. 3 indicated that the changing process for both h_{RW} and g_s roughly fell into two typical periods of recovery (until the peak after irrigation) and stress (from the peak to next irrigation) in each watering-drying cycle. Using Eqs. (16) and (17), the relationship between water stress recovery coefficient δ and $PWDI_{t-1}$ (representing the extent of water stress suffered on the previous day) was investigated in terms of the two periods. During the recovery period with relatively high soil matric potential after irrigation, the root-weighted response function $f(h)$ (i.e. $\int_0^1 f(h)L_{nrd}(z_r)\mathrm{d}z_r$) was kept close to the maximal value of 1, thus δ was able to be approximated as current measured g_s/g_{s0} (i.e. $(g_s/g_{s0})_t$) through combining Eqs. (11) and (12). The relationship between δ (= $(g_s/g_{s0})_t$) and $PWDI_{t-1}$ (= 1-$(g_s/g_{s0})_{t-1}$) under treatments W2-W5 in Exp. 1 showed that δ decreased with increasing $PWDI_{t-1}$ (Fig. 5a), with fitted value of μ = 0.35 (R^2 = 0.65, P < 0.001) for Eq. (16).

In addition, the relationship between δ and $PWDI_{t-1}$ during the stress period with $f(h) < 1$ was analyzed according to the following procedure. (1) Optimizing the fitting parameter ρ in $f(h)$ through combining Eqs. (11)-(13) and (15): This step was performed based on the assumption of $\delta \approx 1$, which was achieved by choosing the peak points of g_s at the maximum recovery level in various watering-drying cycles for treatments W2-W5 (Fig. 3). Corresponding measured data sets (including g_s/g_{s0}, and distributions of soil matric potential and NRLD) should be considered to be under the condition with vanished or much weakened hysteresis (Wu et al., 2020a), and thus optimization of ρ using the nonlinear least-squares method provides ρ = 0.40 (P < 0.05). (2) Calculating $\int_0^1 f(h)L_{nrd}(z_r)\mathrm{d}z_r$ in Eq. (11): With the optimized ρ, fitted NRLD distribution and measured h profiles during stress period in each watering-drying cycle for W2-W5, $\int_0^1 f(h)L_{nrd}(z_r)\mathrm{d}z_r$ were numerically calculated with the trapezoidal formula for next step. (3) Analyzing the relationship between δ and $PWDI_{t-1}$: δ was estimated using the calculated $\int_0^1 f(h)L_{nrd}(z_r)\mathrm{d}z_r$ and measured g_s/g_{s0} through Eqs. (11) and (12), and then correlated with $PWDI_{t-1}$ during stress periods for treatments W2-W5 (Fig. 5b). The fitted result showed that Eq. (16) provided a good compatibility between δ and $PWDI_{t-1}$ with an index of μ = 0.33 (R^2 = 0.37, P < 0.05). Similarly fitted values of μ for both recovery (0.35) and stress (0.33) periods suggested that the quantitative relationship represented by Eq. (16) was robust, independent of the soil water deficit level. Therefore, all the data during both periods were pooled together and yielded an assembling fitting result of μ = 0.34 (R^2 = 0.59, P < 0.001, Fig. 5c).

Pooled retrieved data sets from the literature resulted in relationships between δ (= $(g_s/g_{s0})_t$) and $PWDI_{t-1}$ (= 1 - $(g_s/g_{s0})_{t-1}$) during recovery periods for olive, grape, rockrose, oak, kidney bean, leucaena, thuja, tomato, maize, acacia, tobacco and populus (Fig. 6a-6l). Similar to Fig. 5a, the water stress recovery coefficient δ was negatively correlated with the extent of water stress suffered on the previous day $PWDI_{t-1}$ for all the selected species, and Eq. (16) was successful in fitting these relationships, with R^2 ranging from 0.63 (tobacco, Fig. 6k) to 0.91 (thuja, Fig. 6g). The fitting parameter μ varied widely among species from 0.31 to 0.81, with a mean (MN) of 0.62 and a coefficient of variation (CV) of 0.25. The difference in the parameter μ among species would be attributable to differences in genetic characteristics and growing environments. However, there were small differences for the parameter μ between/among some species, such as olive and grape (MN = 0.81; CV = 1%, Fig. 6a-6b), rockrose, oak, kidney bean, leucaena, thuja, tomato and maize (MN = 0.67; CV = 6%, Fig. 6c-6i), and tobacco and populus (MN = 0.33; CV = 13%, Fig. 6k-6l). Despite the differences in the parameter μ among species, the significant relationships between δ and $PWDI_{t-1}$ further verified the effect of previous water stress on g_s, reasonably described by Eq. (16), a simple power function.

3.2 Estimation of leaf stomatal conductance (Exp. 1)

When the index ρ of $f(h)$ in Eq. (15) and μ of δ in Eq. (16) were known, leaf stomatal conductance g_s under each deficit irrigation treatment in Exp. 1 could be estimated by Eq. (12) using the measured g_s from full irrigation treatment W1 as a reference g_{s0}. To keep independence, the data from treatments W2 and W4 were chosen for parameter optimization, and the remaining data from treatments W3 and W5 were used for verification.

With the fitted NRLD, measured g_s/g_{s0} and distributions of soil matric potential under W2 and W4 in Exp. 1, the parameters ρ and μ were optimized with the nonlinear least squares method as: ρ = 0.43, μ = 0.36 through minimizing the difference between the measured and estimated g_s. Thereafter, the improved g_s model with the optimized parameters was used to estimate g_s of treatment W3 and W5. Meanwhile for comparison, the dynamics of g_s were also estimated using the traditional Jarvis model (i.e. Eq. (6)) with linear response function and averaged root-zone soil matric potential h_{ave} (Eq. (10)). Compared to the traditional model, the improved model provided better estimation results for both parameter optimization and verification processes from different treatments (Fig. 7 and Table 2). As for optimization, the root mean squared error (RMSE), the determination coefficient (R^2) and the Nash-Sutcliffe efficiency coefficient (NSE) between the measured and estimated g_s by the improved model were 0.0006 m s^{-1}, 0.89 and 0.88, respectively, which were all superior to those by the traditional model (RMSE = 0.0019 m s^{-1}, R^2 = 0.75, NSE = -0.26). Similar superiority was observed for verification, with RMSE decreased from 0.002 (by traditional model) to 0.0005 m s^{-1} (improved model), R^2 increased from 0.81 to 0.92 and NSE increased from -0.25 to 0.91.

To demonstrate overall performance, the estimated g_s, under all treatments W2-W5 employed for both optimization and verification, were pooled together, compared with the measurements, and shown in Fig. 8a and 8b, respectively for the traditional and improved models. In general, the improved model significantly enhanced the estimation accuracy of g_s, with 70% decrease of RMSE, 15% increase of R^2 and 1.13 increment of NSE. Therefore, through considering the effects of the relative distribution of soil water to roots, soil water stress hysteresis, and nonlinear characteristics of stomatal response to soil water deficit, the improved soil water stress index significantly enhanced the estimation accuracy of g_s, suggesting that the incorporation of ω into the Jarvis model should be reasonable and reliable.

3.3 Estimation of canopy stomatal conductance (Exp. 2)

As shown in Eq. (6), besides soil water deficit, g_s is also influenced by meteorological factors such as solar radiation R_s, air temperature T and water vapor pressure deficit D in the field lysimetric experiment (Exp. 2). By assuming ω = 1 and thus eliminating the influence of soil water stress for the full irrigation treatment WT0, the three weather dependent parameters k_{Rs}, k_T, k_D were optimized as: k_{Rs} = 119, k_T = 0.021, k_D = 0.001 (P < 0.05), by minimizing the residual between the measured (inversely calculated using the P-M model and measured ET) and estimated g_c. The data from treatments WT1 and WT3 were then used to optimize two water stress dependent parameters ρ and μ for the improved model, and data from treatments WT2 and WT4 used to validate the optimization results.

Based on Eq. (14), the generalized NRLD from Zuo et al. (2013), measured g_c and distributions of soil matric potential under WT1 and WT3 in Exp. 2, the parameters ρ and μ were optimized as: ρ = 0.77, μ = 0.31. Thus, the improved model for winter wheat in Exp. 2 was used to estimate g_c under treatments WT2 and WT4. The estimated g_c by both improved and traditional g_c models was compared with the measured values (Fig. 9 and Table 2). The estimated g_c by the improved model matched well with the measured values, with RMSE ≤ 0.002 m s^{-1}, but R^2 ≥ 0.66 and NSE ≥ 0.66 for both optimization and verification treatments. The traditional model (with RMSE ≤ 0.0028 m s^{-1}, R^2 ≥ 0.61, NSE ≥ 0.32) was less successful. Hence, the general estimation results by the improved Jarvis model also demonstrated a better performance with 27% decrease of RMSE, and 2% (0.27) increase of R^2 (NSE), respectively, for estimating g_c compared to those by traditional model (Fig. 10).

3.4 Estimation of cumulative evapotranspiration (Exp. 3)

In order to further test the applicability of the improved Jarvis g_c model under different environments, it was coupled with the P-M model and used to estimate cumulative ET (CET) of winter wheat during different growing stages in the field drip irrigation experiment (Exp. 3). The P-M model was established by optimizing five fitting parameters, i.e. k_{Rs}, k_T, k_D, ρ and μ, according to the procedure as follows:

(1) Choosing full water supply duration to simulate optimal soil water condition and conducting water balance analysis through Eq. (1) to obtain potential CET: Since a heavy rainfall of 35 mm fell on 217 DAS (Fig. 1b), the follow-up period of 218-225 DAS (corresponding to the filling stage) was assumed to be under optimal soil water condition, and correspondingly, the potential CET of winter wheat at this duration under each treatment (T1-T4) was calculated through water balance (Table 3).

(2) Optimizing the weather dependent parameters in Eq. (6): Based on the assumption of ω = 1, and the measured potential CET, LAI and daily meteorological data during 218-225 DAS, the weather dependent parameters k_{Rs}, k_T, k_D were optimized as: k_{Rs} =1005; k_T = 0.014; k_D = 0.001 (P < 0.05), by minimizing the residual between the measured and estimated potential CET.

(3) Optimizing the two water stress dependent parameters ρ and μ in Eqs. (15) - (16): The field water balance interval is usually set to be not less than 5 d due to the fact that the accuracy of water balance would decrease with decreasing balance interval and the influence of uncertainty in water balance would sharply increase when the interval is less than 5 d (Rana and Katerji, 2000). Therefore, the water treatment period eliminating the full water supplied duration (218-225 DAS) was divided into five sequential balance stages (i.e. 197-204, 204-211, 211-218, 225-232 and 232-239 DAS) with identical interval of 7 d, in which the actual CET under each

treatment was analyzed using Eq. (1) and shown in Table 3. Then, the water stress related parameters ρ and μ were optimized as: ρ = 0.50 and μ = 0.40 using relevant data from treatments T1 and T3. A corresponding optimization process produced RMSE, R^2 and NSE between measured and estimated actual CET using both improved and traditional models as shown in Table 2.

The actual CET during each balance stage under verification treatments T2 and T4 in Exp. 3 was estimated using the improved and traditional methods. The RMSE, R^2 and NSE between the measured (calculated through water balance using measured soil water information) and estimated CET by the improved and traditional P-M models are compared in Table 2. The estimated CET by the improved P-M model better agreed with the measured values in comparison to the traditional model, with RMSE decreasing to 8.2 mm from 14.1 mm, R^2 (NSE) increasing to 0.67 (-1.48) from 0.56 (0.15) for the verification treatments. The overall estimation results of CET for both optimization and verification treatments showed that RMSE was reduced by 42% and R^2 (NSE) increased by 17% (1.5), when comparing the new model to the traditional model (Fig. 11). Therefore, the P-M model by coupling the improved g_c model was still reliable and stable in estimating ET for different field environments.

3.5 Overview of estimations

When the traditional model was employed, estimated g_s (Fig. 8a), g_c (Fig. 10a), and CET (Fig. 11a) tended to be higher than the corresponding measured values, especially for g_s in Exp. 1 (Fig. 8a) and CET in Exp. 3 (Fig. 11a). This is likely due to the underestimation of water stress effect (extent) on stomatal conductance using a linear response function $f(h_{ave})$, leading to higher stomatal conductance and ET. For example, corresponding to a fixed h_{RW}, the fitted relative g_s by the linear function $f(h_{ave})$ was always higher than the measured values (Fig. 4). The overestimation of both stomatal conductance and ET was much alleviated by substituting $f(h_{ave})$ with ω, in which the extent of water stress was dependent on current soil water availability represented by the integral $\int_0^1 f(h) L_{nrd}(z_r)\,\mathrm{d}z_r$ (combining effects of both nonlinear response function $f(h)$ and its relative distribution to NRLD), as well as on water stress hysteresis effect represented by δ. In Exps.1-3, the optimized parameters ρ of $f(h)$ were all less than 1 (i.e. 0.43; 0.77; 0.50), presenting concave shapes and the features of relatively more serious water stress compared to the linear function (Homaee et al., 2002; Rallo and Provenzano, 2013), especially for the cases with lower ρ, e.g. Exp. 1 and Exp. 3. As shown in Fig. 4, the relative g_s fitted by concave nonlinear response function was much closer to the measured relative g_s, both of which were always lower than that produced by the linear response function. Soil water availability is also closely related to the relative distribution relationship between soil water to roots (Gardner, 1960; Shi et al., 2015), which changes greatly with changing distributions of soil matric potential along a soil profile due to irrigation/rainfall and evapotranspiration. If the distribution of soil matric potential coincides with that of NRLD (Case 1: often occurring shortly after irrigation/rainfall), more water is located in the upper soil layers with more roots, thus benefiting plant water use, and leading to greater stomatal aperture. Conversely, if the distributions of soil matric potential and NRLD do not coincide with each other (Case 2: often occurring during drought periods), root zone available water is reduced so as to induce water stress and stomatal limitation. In Exps.1-3, the prolonged drought (Case 2) was very common due to deficit irrigation and/or limited rainfall, thus winter wheat was exposed to relatively serious water stress as the consequence of the mismatch from distributions between soil matric potential and NRLD. In such case, water stress extent would be generally underestimated when using $f(h_{ave})$ rather than ω, because the averaged soil matric potential h_{ave} magnified the availability of water in the deeper zone with fewer roots. Moreover, the recovery of g_s after re-watering was reported to be negatively related to the degree of previous water stress (Resco et al., 2008; Torres-Ruiz et al., 2014). Ignoring the water stress hysteresis effect would also result in overestimated g_s and ET (Wu et al., 2020a, b), which could be offset by the introduction of δ justified in this study (Figs. 5 and 6).

Two additional fitting parameters ρ and μ were required in ω. To test their sensitivity to the Jarvis and/or P-M model, the relative changes in estimating g_s (Exp. 1), g_c (Exp. 2) and CET (Exp. 3) were evaluated by fluctuating the parameters with ± 10% and ± 30% errors. The results showed that the estimated g_s, g_c and CET increased with increasing ρ or decreasing μ, and were more sensitive to ρ compared than to μ (Table 4). Fluctuating ρ (μ) by ± 10% and ± 30% resulted in changes of g_s within ± 5.6% (± 2.6%) and ± 19.0% (± 8.2%) in Exp. 1, g_c within ± 6.2% (± 2.8%) and ± 19.9% (± 8.8%) in Exp. 2, and CET within ± 3.9% (± 1.8%) and ± 13.9% (± 5.8%) in Exp. 3. In general, the relative estimation error caused by 10% fluctuation of the parameters was restrained to within 7%, and that by 30% fluctuation to within 20%, indicating that the uncertainty in parameters ρ and μ would have relatively small influence on the estimation of stomatal conductance and ET.

Taking the intrinsic soil-plant water relations including the effects of the relative distribution of soil water to roots and water stress hysteresis on g_s, and the nonlinear stomatal response to soil water deficit into consideration, the improved index ω was found to be reasonable and reliable in characterizing soil water stress. As for the construction of ω, the indispensable NRLD distribution, showing a general trend regardless of soil environment, species, growing season, climate, or other factors, is often statistically generalized as a function like Eq. (13) or (14) for a specific plant, e.g. wheat, cotton, maize, rice, or beans (Zuo et al., 2013; Ning et al., 2015, 2019).

The nonlinear response function, another critical variable in ω, can be expressed in different forms such as concave/convex (Lhomme et al., 1998; Musters and Bouten 1999; Steduto et al., 2009; Rallo and Provenzano 2013) and S-shaped (van Genuchten 1987; Dirksen et al., 1993; Homaee et al., 2002). Accurate estimation of stomatal conductance may be dependent on the selection of an appropriate function (Wang et al., 2014). Obviously, the arbitrarily selected piecewise power response function in this study needs further evaluation and comparison with other various response functions. Furthermore, a number of complicated physiological, biochemical and hydraulic factors are involved in water stress hysteresis or recovery (Chaves et al., 2009; Torres-Ruiz et al., 2014), and thereby an integrated understanding of stomatal regulation in response to the stress-recovery cycle remains elusive. This work verifies the feasibility of a recently proposed empirical water stress recovery coefficient δ in quantifying the stress hysteresis, which should be further examined and evaluated under more wide and complicated environmental conditions.

4. Conclusions

A novel soil water stress index was introduced into the Jarvis model to improve the representation of stomatal response to drought stress. More complete soil-plant water relations, including the effects of relative distribution of soil water to roots and water stress hysteresis on g_s, as well as the nonlinear stomatal response to soil water deficit, were taken into consideration in the improvements. The index ω was employed to estimate stomatal conductance and evapotranspiration through Jarvis and P-M models. To verify the relationships between leaf stomatal conductance g_s and root-zone soil water status, and the extent of water stress previously suffered by plants, and to test and evaluate the accuracy and reliability of ω, a greenhouse and two field experiments (lysimetric and drip-irrigated) for winter wheat were conducted. Results from greenhouse experiment showed that the nonlinear response function was superior to the linear function in describing the descending process of g_s with decreasing root-weighted soil matric potential. The relationship between g_s and previous water stress extent was found to be feasibly generalized as a power function, which was further verified and confirmed by the retrieved measured data from literature. Comparing with the traditional model (based on linear response function $f(h_{ave})$), the improved model (based on ω) significantly enhanced the estimation accuracy of g_s, g_c, and CET, and yielded corresponding RMSE between estimated and measured values less than 0.0006 m s^{-1}, 0.0020 m s^{-1}, and 8.2 mm, and R^2 (NSE) greater than 88% (0.87), 65% (0.65), and 66% (0.14), respectively. The improved soil water stress index should be helpful for rationally characterizing stomata physiological responses to water stress, and accurately estimating the stomatal conductance and evapotranspiration. However, appropriate selection of nonlinear response function, and justification of ω under widely varying environments still need further research.

Acknowledgments

This research was supported partly by National Natural Science Foundation of China (U1706211, 51790532), National Key Research and Development Program of China (2016YFD0200303, 2017YFE0118100), and the European Union's Horizon 2020 research and innovation programme under Project SHui, grant agreement No 773903.

References

Arora, V.K., 2003. Simulating energy and carbon fluxes over winter wheat using coupled land surface and terrestrial ecosystem models. Agric. Forest Meteorol. 118, 21-47.

Bai, Y., Li, X., Liu, S., Wang, P., 2017. Modelling diurnal and seasonal hysteresis phenomena of canopy conductance in an oasis forest ecosystem. Agric. For. Meteorol. 246, 98-110.

Bengtson, C., Falk, S.O., Larsson, S., 1977. The after-effect of water stress on transpiration rate and changes in abscisic acid content of young wheat plants. Physiol. Plant. 41, 149-154.

Ben-Mehrez, M., Taconet, O., Vidal-Madjar, D., Valencogne, C., 1992. Estimation of stomatal resistance and canopy evaporation during the HAPEX-MOBILHY experiment. Agric. For. Meteorol. 58, 285-313.

Blackman, C.J., Brodribb, T.J., Jordan, G.J., 2009. Leaf hydraulics and drought stress: response, recovery and survivorship in four woody temperate plant species. Plant Cell Environ. 32, 1584-1595.

Boussiba, S., Richmond, A.E., 1976. Abscisic acid and the after-effect of stress in tobacco plants. Planta 129, 217-219.

Cai, G.C., Vanderborght, J., Couvreur, V., Mboh, C.M., Vereecken, H., 2017. Parameterization of root water uptake models considering dynamic root distributions and water uptake compensation. Vadose Zone J. 17, 160125. https://doi.org/10.2136/vzj2016.12.0125

Chaves, M.M., Flexas, J., Pinheiro, C., 2009. Photosynthesis under drought and salt stress: regulation mechanisms from whole plant to cell. Ann. Bot. 103, 551-560.

Chen, J.W., Zhang, Q., Li, X.S., Cao, K.F., 2010. Gas exchange and hydraulics in seedlings of *hevea brasiliensis* during water stress and recovery. Tree Physiol. 30, 876-885.

Comstock, J.P., 2002. Hydraulic and chemical signalling in the control of stomatal conductance and transpiration. J. Exp. Bot. 53, 195-200.

Damour, G., Simonneau, T., Cochard, H., Urban, L., 2010. An overview of models of stomatal conductance at the leaf level. Plant. Cell. Environ. 33, 1419-1438.

Dirksen, C., Kool, J.B., Koorevaar, P., Van Genuchten, M.T., 1993. HYSWASOR-simulation model of hysteretic water and solute transport in the root zone. In: Russo, D., Dagan, G. (Eds.), Water Flow and Solute Transport in Soils. Springer Verlag, New York, pp. 99-122.

Dörffling, K., Streich, J., Kruse, W., Muxfeldt, B., 1977. Abscisic acid and the after-effect of water stress on stomatal opening potential. Z. Pflanzenphysio. 81, 43-56.

Dry, P.R., Loveys, B.R., 1999. Grapevine shoot growth and stomatal conductance are reduced when part of the root system is dried. Vitis 38, 151-156.

Egea, G., Verhoef, A., Vidale, P.L., 2011. Towards an improved and more flexible representation of water stress in coupled photosynthesis-stomatal conductance models. Agric. For. Meteorol. 151, 1370-1384.

Feddes, R.A., Kowalik, P.J., Malinka, K.K., Zaradny, H., 1976. Simulation of field water uptake by plants using a soil water dependant root extraction function. J. Hydrol. 31, 13-26.

Fischer, R.A., Hsiao, T.C., Hagan, R.M., 1970. After-effect of water stress on stomatal opening potential: I techniques and magnitudes. J. Exp. Bot. 2, 371-385.

Flexas, J., Bota, J., Cifre, J., Escalona, J.M., Galmés, J., Gulías, J., Lefi, E., MartetínezCanellas, S.F., Moreno, M.T., Ribas-Carbó, M., Riera, D., Sampol, B., Medrano, H., 2004. Understanding down-regulation of photosynthesis under water stress: future prospects and searching for physiological tools for irrigation management. Ann. Appl. Biol. 144, 273-283.

Galle, A., Florez-Sarasa1, I., Aououad, H.E., Flexas, J., 2011. The Mediterranean evergreen *Quercus ilex* and the semi-deciduous *Cistus albidus* differ in their leaf gas exchange regulation and acclimation to repeated drought and re-watering cycles. J. Exp. Bot. 62, 5207-5216.

Galmés, J., Medrano, H., Flexas, J., 2007. Photosynthetic limitations in response to water stress and recovery in Mediterranean plants with different growth forms. New Phytol. 175, 81-93.

Gardner, W.R., 1960. Dynamic aspect of water availability to plants. Soil Sci. 89, 63-73.

Guswa, A.J., Celia, M.A., Rodriguez-Iturbe, I., 2004. Effect of vertical resolution on predictions of transpiration in water-limited ecosystems. Adv. Water Resour. 27, 467-480.

Hasegawa, S., Eguchi, S., 2002. Soil water conditions and flow characteristics in the subsoil of a volcanic ash soil: Findings from field monitoring from 1997 to 1999. Soil Sci. Plant Nutr. 48, 227-236.

Homaee, M., Feddes, R.A., Dirksen, C., 2002. Simulation of root water uptake. II. Nonuniform transient water stress using different reduction functions. Agric. Water Manage. 57, 111-126.

Iovieno, P., Punzo, P., Guida, G., Mistretta, C., Van Oosten, M. J., Nurcato, R., Bostan, H., Colantuono, C., Costa1, A., Bagnaresi, P., Chiusano, M., Albrizio, R., Giorio, P., Batelli, G., Grillo, S., 2016. Transcriptomic changes drive physiological responses to progressive drought stress and rehydration in tomato. Front. Plant Sci. 7, 371.

Izanloo, A., Condon, A.G., Langridge, P., Tester, M., Schnurbusch, T., 2008. Different mechanisms of adaptation to cyclic water stress in two South Australian bread wheat cultivars. J. Exp. Bot. 59, 3327-3346.

Jarvis, P.G., 1976. The interpretation of the variations in leaf water potential and stomatal conductance found in canopies in the field. Philos. Trans. R. Soc. B: Biol. Sci. 273, 593-610.

Jin, J.Q., Guo, Q.S., Zhu. L., Xu, G.X., Liu, J.F., Pei, S.X., 2012. Effects of drought and rewatering photosynthetic characteristics and water use efficiency of Cypresses arborvitae. Plant sci. 30, 599-610. (in Chinese with English Abstract)

Keenan, T., Sabate, S., Gracia, C., 2010. Soil water stress and coupled photosynthesis conductance models: bridging the gap between conflicting reports on the relative roles of stomatal, mesophyll conductance and biochemical limitations to photosynthesis. Agric. For. Meteorol. 150, 443-453.

Lhomme, J.P., Elguero, E., Chehbouni, A., Boulet, G., 1998. Surface water and climate-stomatal control of transpiration: examination of Monteith's formulation of canopy resistance. Water Resour. Res. 34, 2301-2308.

Li, S., Hao, X., Du, T., Tong, L., Zhang, J., Kang, S., 2013. A coupled surface resistance model to estimate crop evapotranspiration in arid region of northwest China. Hydrol. Processes 28, 2312-2323.

Li, X., Kang, S., Niu, J., Huo, Z., Liu, J., 2019. Improving the representation of stomatal responses to CO_2 within the Penman-Monteith model to better estimate evapotranspiration responses to climate change. J. Hydrol. 572, 692-705.

Liang, J.S., Zhang, J.H., 1999. The relations of stomatal closure and reopening to xylem ABA concentration and leaf water potential during soil drying and rewatering. Plant Growth Regul. 29, 77-86.

Liu, C., Li, Z., Yang, K., Xu, J., Wang, Y., Zhang, C., et al. 2015. Effects of water stress and subsequent rehydration on physiological characteristics of maize (*Zea mays*) with different drought tolerance. J Plant Physiol. 51, 702-708. (in Chinese with English Abstract)

Mahfouf, J.F., Ciret, C., Ducharne, A., Irannejad, P., Noilhan, J., Shao, Y., Thornton, P., Xue, Y., Yang, Z.L., 1996. Analysis of transpiration results from the RICE and PILPS workshop. Global Planet. Change 13, 73-88.

Marron, N., Delay, D., Petit, J.M., Dreyer, E., Kahlem, G., Delmotte, F., Brignolas, F., 2002. Physiological traits of *Populus* × *euramericana* cloes luisa avanzo and dorskamp, during a water stress and re-watering cycle. Tree Physiol. 22, 849-858.

Misson, L., Panek, J.A., Goldstein, A.H., 2004. A comparison of three approaches to modeling leaf gas exchange in annually drought-stressed ponderosa pine forests. Tree Physiol. 24, 529-541.

Miyashita, K., Tanakamaru, S., Maitani, T., Kimura, K., 2005. Recovery responses of photosynthesis,transpiration, and stomatal conductance in kidney bean following drought stress. Environ. Exp. Bot. 53, 205-214.

Monteith, J.L., 1965. Evaporation and environment. In: Fogg, B.D. (Ed.), The State and Movement of Water in Living Organism. Symposia Soc. Exp. Biol. pp. 205-234.

Musters, P.A.D., Bouten, W., 1999. A method for identifying optimum strategies of measuring soil water contents for calibrating a root water uptake model. J. Hydrol. 227, 273-286.

Ning, S., Chen, C., Zhou, B., Wang, Q., 2019. Evaluation of normalized root length density distribution models. Field Crops Res. 242, 107604.https://doi.org/10.1016/j.fcr.2019.107604

Ning, S., Shi, J., Zuo, Q., Wang, S., Ben-Gal, A., 2015. Generalization of the root length density distribution of cotton under film mulched drip irrigation. Field Crops Res. 177, 125-136.

Nortes, P.A., Pérez-Pastor, A., Egea, G., Conejero, W., Domingo, R., 2005. Comparison of changes in stem diameter and water potential values for detecting water stress in young almond trees. Agric. Water Manage. 77, 296-307.

Ogle, K., Barber, J.J., Barron-Gafford, G.A., Bentley, L.P., Young, J.M., Huxman, T.E., Loik, M.E., Tissue, D.T., 2015. Quantifying ecological memory in plant and ecosystem processes. Ecol. Lett. 18, 221-235.

Ono, K., Maruyama, A., Kuwagata, T., Mano, M., Takimoto, T., Hayashi, K., Hasegawa, T., Miyata, A., 2013. Canopy-scale relationships between stomatal conductance and photosynthesis in irrigated rice. Global Change Biol. 19, 2209-2220.

Perez-Martin, A., Michelazzo, C., Torres-Ruiz, J.M., Flexas, J., Fernández, J.E., Sebastiani, L., Diaz-Espejo, A., 2014. Regulation of photosynthesis, stomatal and mesophyll conductance under water stress acclimation and recovery in olive trees: correlation with gene expression of carbonic anhydrase and aquaporins. J Exp Bot 65, 3143-3156.

Porporato, A., Laio, F., Ridolfi, L., Rodriguez-Iturbe, I., 2001. Plants in water-controlled ecosystems: active role in hydrologic processes and response to water stress III. Vegetation water stress. Adv. Water Resour. 24, 725-744.

Pou, A., Flexas, J., Alsina, M.M., Bota, J., Carambula, C., de Herralde, F., 2008. Adjustments of water use efficiency by stomatal regulation during drought and recovery in the drought-adapted *Vitis* hybrid Richter-110 (V. *Berlandieri* × V. *Rupestris*). Physiol. Plantarum 134, 313-323.

Pou, A., Flexas, J., Martorell, S., Tomàs, M., Medrano, H., 2012. Water use efficiency during drought and recovery in grapevines: Differential behaviour of three cultivars. Acta Hort. 931, 127-135.

Rallo, G., Provenzano, G., 2013. Modelling eco-physiological response of table olive trees (*Olea europaea* L.) to soil water deficit conditions. Agric. Water Manag. 120, 79-88.

Rana, G., Katerji, N., 2000. Measurement and estimation of actual evapotranspiration in the field under Mediterranean climate: A review. Eur. J. Agron. 13, 125-153.

Resco, V., Ewers, B.E., Sun, W., Huxman, T.E., Weltzin, J.F., Williams, D.G., 2008. Drought-induced hydraulic limitations constrain leaf gas exchange recovery after precipitation pulses in the C3 woody legume, *Prosopis velutina*. New Phytol. 181, 672-682.

Sanchez, R.A., Hall, A.J., Trapani, N., Hunau, R.C.D., 1983. Effects of water stress on the chlorophyll content, nitrogen level and photosynthesis of leaves of two maize genotypes. Photosynthesis Res. 4, 35-47.

Sellers, P.J., Randall, D.A., Collatz, G.J., Berry, J.A., Field, C.B., Dazlich, D.A., Zhang, C., Collelo, G.D., Bounoua, L., 1996. A revised land surface parameterization (SiB2) for atmospheric GCMs. Part I. Model formulation. J. Climate 9, 676-705.

Shi, J.C., Li, S., Zuo, Q., Ben-Gal, A., 2015. An index for plant water deficit based on root-weighted soil water content. J. Hydrol. 522, 285-294.

Shi, J.C., Yasuor, H., Yermiyahu, U., Zuo, Q., Ben-Gal, A., 2014. Dynamic responses of wheat to drought and nitrogen stresses during re-watering cycles. Agric. Water Manage. 146, 163-172.

Šimůnek, J., Hopmans, J.W., 2009. Modeling compensated root water and nutrient uptake. Ecol. Model. 220, 505-521.

Souza, R.P., Machado, E.C., Silva, J.A.B., Lagoa, A.M.M.A., Silveira, J.A.G., 2004. Photosynthetic gas exchange, chlorophyll fluorescence and some associated metabolic changes in cowpea (*Vigna unguiculata*) during water stress and recovery. Environ. Exp. Bot. 51, 45-56.

Stalfelt, M.G., 1955. The stomata as a hydrophotic regulator of the water deficit of the plant. Physiol. Plantarum 8, 572-593.

Steduto, P., Hsiao, T.C., Raes, D., Fereres, E., 2009. Aquacrop-The FAO crop model to simulate yield response to water: I. concepts and underlying principles. Agron. J. 101, 426-437.

Stewart, J.B., 1988. Modeling surface conductance of pine forest. Agric. For. Meteorol. 43, 19-35.

Tardieu, F., Parent, B., Simonneau, T., 2010. Control of leaf growth by abscisic acid: hydraulic or non-hydraulic processes? Plant Cell Environ. 33, 636-647.

Thom, A.S., 1972. Momentum, mass and heat exchange of vegetation. Q. J. R. Meteorol. Soc. 98, 124-134.

Torrecillas, A., Guillaumeb, C., Alarcon, J., Ruiz-sanchez, M., 1995. Water relations of two tomato species under water stress and recovery. Plant Sci. 105, 169-176.

Torres-Ruiz, J.M., Diaz-Espejo, A., Perez-Martin, A., Hernandez-Santana, V., 2014. Role of hydraulic and chemical signals in leaves, stems and roots in the stomatal behaviour of olive trees under water stress and recovery conditions. Tree Physiol. 35, 415-424.

van Genuchten, M.T., 1980. A closed-form equation for predicting the hydraulic conductivity of unsaturated soils. Soil Sci. Soc. Am. J. 44, 892-898.

van Genuchten, M.T., 1987. A numerical model for water and solute movement in and below the root zone. Res. Rep., 121, USDAARS, U.S. Salinity Laboratory, Riverside, CA USA.

Virlouvet, L., Fromm, M., 2015. Physiological and transcriptional memory in guard cells during repetitive dehydration stress. New Phytol.205, 596-607.

Wang, H.L., Guan, H., Deng, Z., Simmons, C.T., 2014. Optimization of canopy conductance models from concurrent measurements of sap flow and stem water potential on Drooping Sheoak in South Australia. Water Resour. Res. 50, 6154-6167.

Wraith, J.M., Or, D., 1998. Nonlinear parameter estimation using spreadsheet software. J. Nat. Resour. Life Sci. Educ. 27, 13-19.

Wu, X., Zhang, W.J., Liu, W., Zuo, Q., Shi, J.C., Yan, X., D, Zhang, H.F., Xue, X.Z., Wang, L.C., Zhang, M., Ben-Gal, A., 2017. Root-weighted soil water status for plant water deficit index based irrigation scheduling. Agric. Water Manage. 189, 137-147.

Wu, X., Shi, J.C., Zuo, Q., Zhang, M., Xue, X.Z., Wang, L.C., Zhang, T., Ben-Gal, A., 2020a. Parameterization of the water stress reduction function based on soil–plant water relations. Irri. Sci. https://doi.org/10.1007/s00271-020-00689-w

Wu, X., Zuo, Q., Shi, J.C., Wang, L.C., Xue, X.Z., Ben-Gal, A., 2020b. Introducing water stress hysteresis to the Feddes empirical macroscopic root water uptake model. Agric. Water Manage. 240, 106293. https://doi.org/10.1016/j.agwat.2020.106293

Xu, X., Lin, H., Fu, Z., 2004. Probe into the method of regional ecological rise assessment-a case study of wetland in the yellow river delta in china. J. Environ. Manage. 70, 253-262.

Zuo, Q., Zhang, R., Shi, J., 2013. Characterization of the root length density distribution of wheat using a generalized function. In: Timlin, D., Ahuja, L.R. (Eds.), Enhancing Understanding and Quantification of Soil-Root Growth Interactions. American Society of Agronomy Publisher, pp. 93-117.

Figures

Fig. 1. The dynamics of daily temperature (T), wind speed (u), relative humidity (RH), solar radiation (R_s), and precipitation (P, only included in Exp. 3) from jointing (197 DAS) until mature (243 DAS) of winter wheat in (a) Exp. 2 and (b) Exp. 3. DAS = days after sowing.

Fig. 2. Schematic diagram of drip-irrigated winter wheat planting pattern in Exp. 3 (unit: cm).

Fig. 3. The dynamics of root-weighted soil matric potential (h_{RW}), potential (g_{s0}) and actual (g_s) leaf stomatal conductance of winter wheat during each sampling cycle under treatments (a) W2, (b) W3, (c) W4, and (d) W5 in Exp. 1. Vertical bars indicate standard errors. DAS = days after sowing.

Fig. 4. Measured and (linearly or nonlinearly) fitted relative leaf stomatal conductance (g_s/g_{s0}) as a function of root-weighted soil matric potential (h_{RW}) under W2-W5 treatments in Exp. 1.

Fig. 5. The relationships between the measured or fitted water stress recovery coefficient (δ) and the plant water deficit index on the previous day (PWDI_{t-1}) during (a) recovery, (b) stress, and (c) recovery-stress periods under W2-W5 treatments for winter wheat in Exp. 1.

Fig. 6. The relationships between the measured water stress recovery coefficient δ and the plant water deficit index on the previous day (PWDI_{t-1}) during recovery periods for the retrieved twelve plant species as listed in the following table:

Plant species	References	Plant species	References
(a) Olive	Perez-Martin et al., 2014	(g) Thuja	Jin et al., 2012
(b) Grape	Dry and Loveys, 1999; Flexas et al., 2004; Pou et al., 2012	(h) Tomato	Torrecillas et al., 1995; Iovieno et al., 2016
(c) Rockrose	Galle et al., 2011	(i) Maize	Sanchez et al., 1982; Liu et al., 2015
(d) Oak	Galle et al., 2011	(j) Acacia	Liang and Zhang, 1999
(e) Kidney bean	Miyashita et al., 2005	(k) Tobacco	Fischer et al., 1970; Boussiba and Richmond, 1976
(f) Leucaena	Liang and Zhang, 1999	(l) Populus	Marron et al., 2002

Fig. 7. The dynamics of measured and estimated leaf stomatal conductance (g_s) by traditional or improved Jarvis model during each sampling (or irrigation) cycle under treatments (a) W2 (for

optimization), (b) W3 (for verification), (c) W4 (for optimization), and (d) W5 (for verification) in Exp. 1. Vertical bars indicate standard errors. DAS = days after sowing.

Fig. 8. Comparisons of the estimated leaf stomatal conductance (g_s) by (a) traditional and (b) improved Jarvis models with the measured g_s under treatments W2-W5 in Exp. 1.

Fig. 9. The dynamics of measured canopy stomatal conductance (g_c), inversely calculated from the Penman-Monteith model using the measured evapotranspiration, and the estimated g_c by traditional and improved Jarvis models under treatments (a) WT1 (for optimization), (b) WT2 (for verification), (c) WT3 (for optimization), and (d) WT4 (for verification) in Exp. 2. Vertical bars indicate standard errors. DAS = days after sowing.

Fig. 10. Comparisons of the estimated canopy stomatal conductance (g_c) by (a) traditional and (b) improved Jarvis models with the measured g_c (inversely calculated using Penman-Monteith model and measured evapotranspiration) under treatments WT1-WT4 in Exp. 2.

Fig. 11. Comparisons of the estimated cumulative evapotranspiration (CET) by Penman-Monteith model coupled with (a) traditional and (b) improved Jarvis model with the measured CET (calculated by the water balance method using the measured soil water information) under treatments T1-T4 in Exp. 3.

Fig. 1

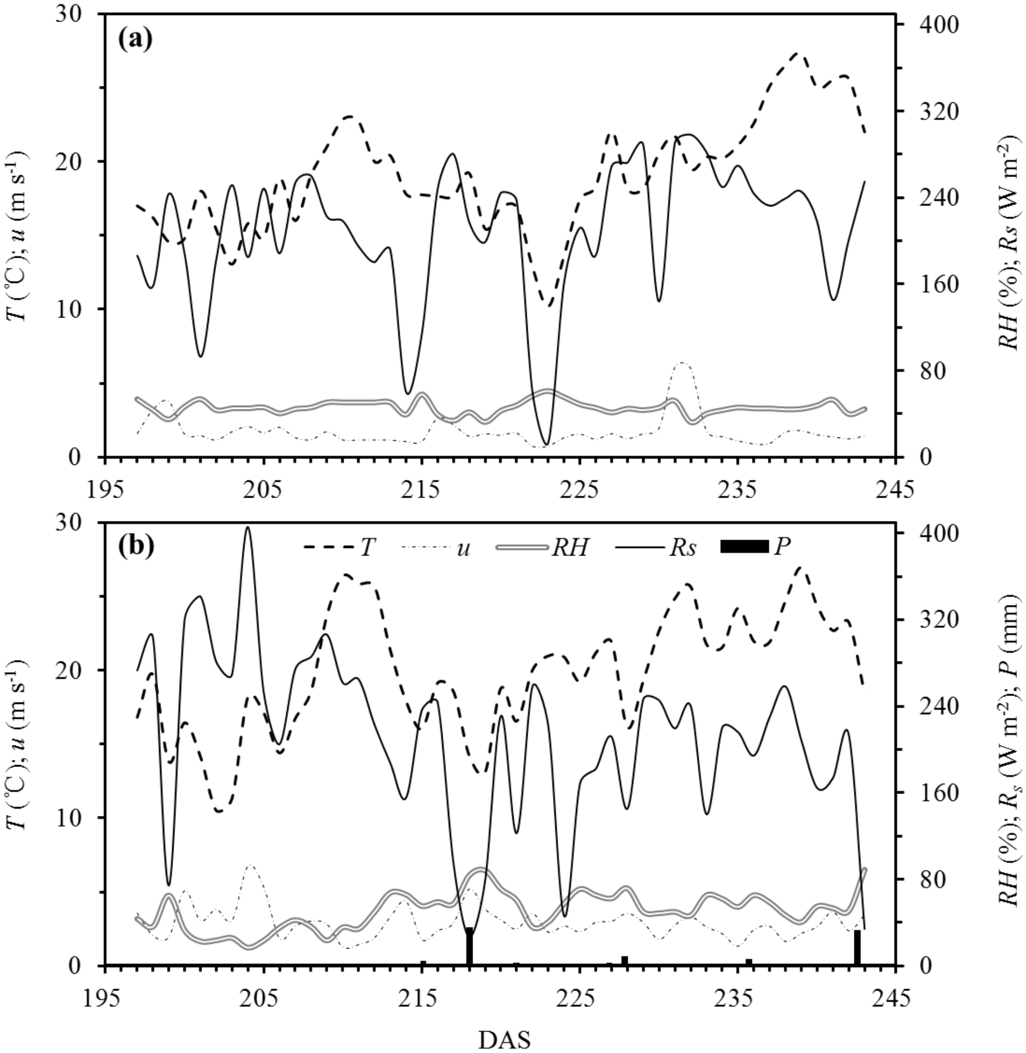
(a)
(b)
T (°C); u (m s-1)
RH (%); Rs (W m-2)
RH (%); Rs (W m-2); P (mm)
T
u
RH
Rs
P
DAS
195
205
215
225
235
245
0
10
20
30
0
80
160
240
320
400

Fig. 2

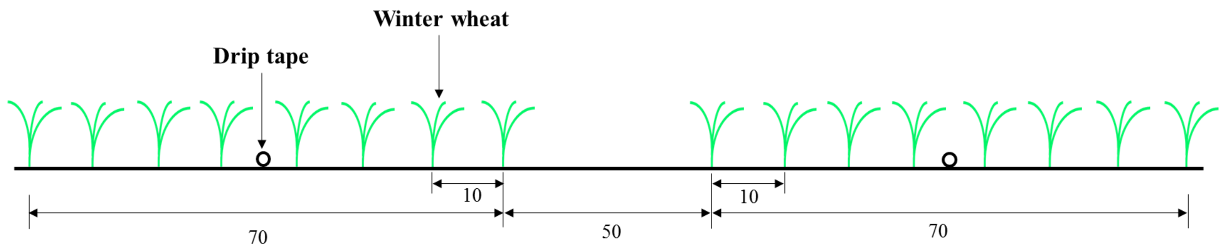

862 **Fig. 3**

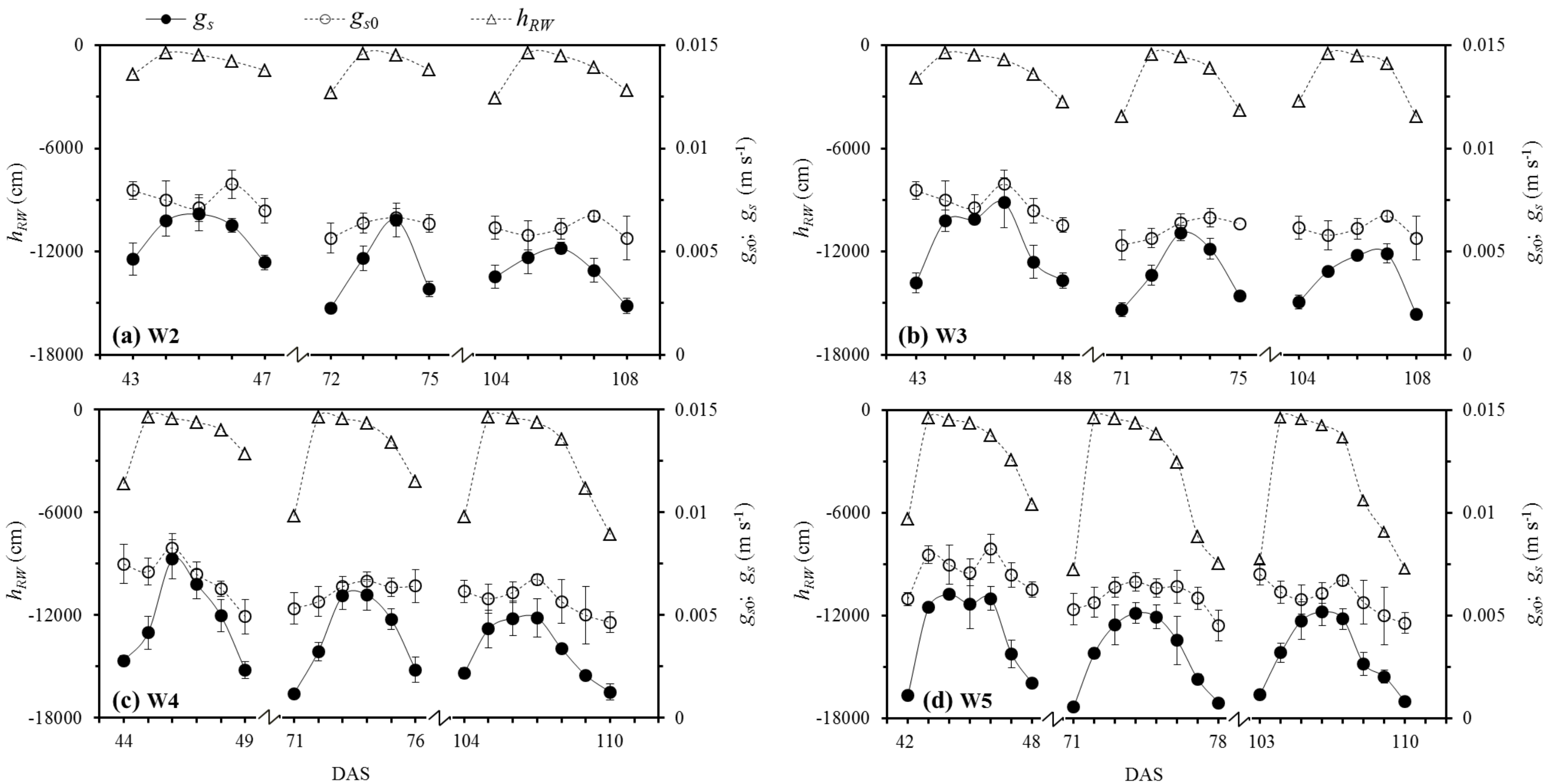
g_s
g_{s0}
h_{RW}
(a) W2
(b) W3
(c) W4
(d) W5
h_{RW} (cm)
g_{s0}; g_s (m s^{-1})
DAS
0
-6000
-12000
-18000
0.015
0.01
0.005
0

863

Fig. 4

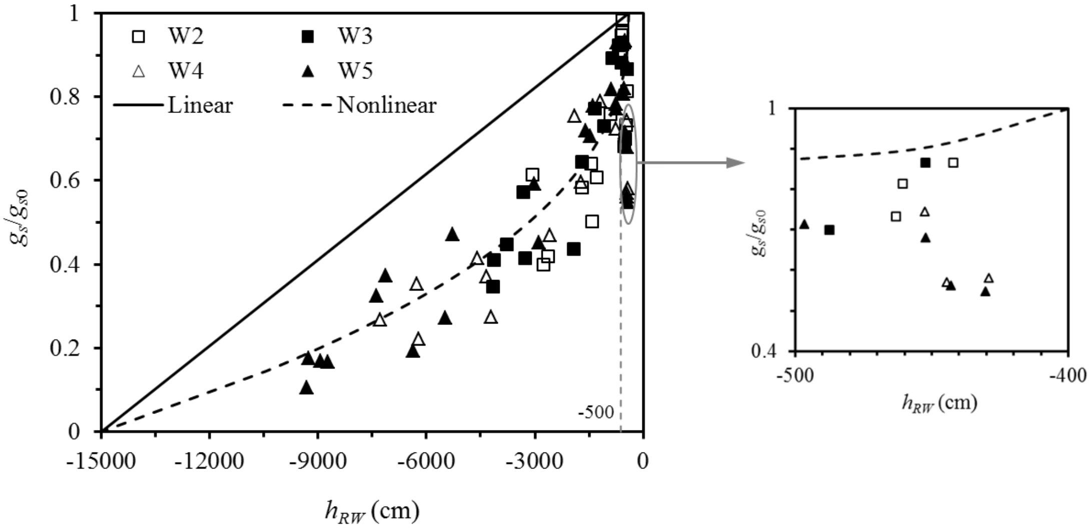

Fig. 5

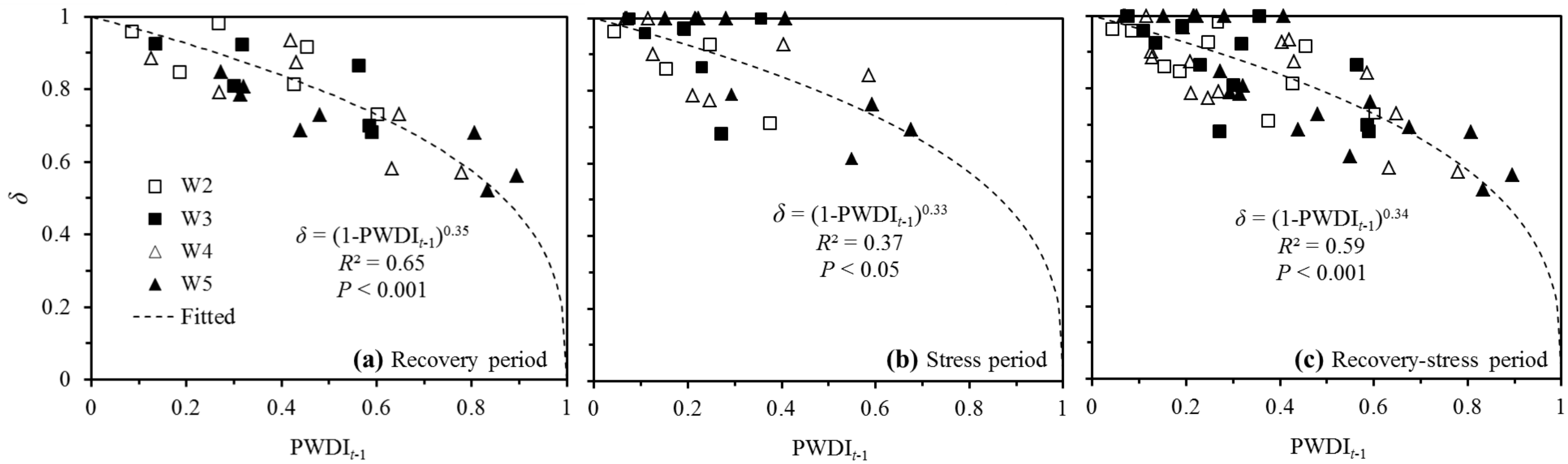
δ
W2
W3
W4
W5
Fitted
δ = (1-PWDI_{t-1})^{0.35}
R² = 0.65
P < 0.001
(a) Recovery period
δ = (1-PWDI_{t-1})^{0.33}
R² = 0.37
P < 0.05
(b) Stress period
δ = (1-PWDI_{t-1})^{0.34}
R² = 0.59
P < 0.001
(c) Recovery-stress period
PWDI_{t-1}
PWDI_{t-1}
PWDI_{t-1}

Fig. 6

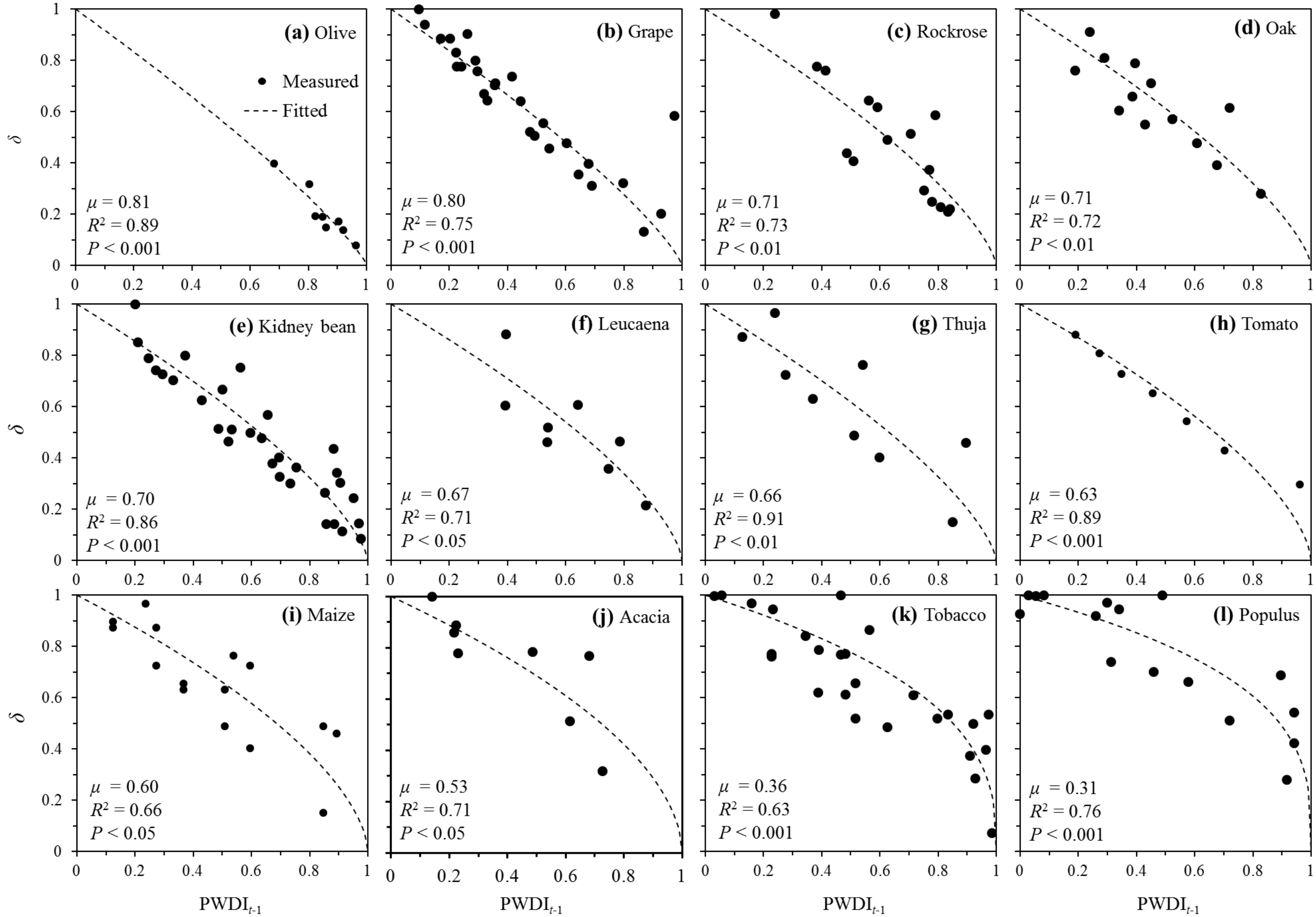

(a) Olive
Measured
Fitted
μ = 0.81
R² = 0.89
P < 0.001
(b) Grape
μ = 0.80
R² = 0.75
P < 0.001
(c) Rockrose
μ = 0.71
R² = 0.73
P < 0.01
(d) Oak
μ = 0.71
R² = 0.72
P < 0.01
(e) Kidney bean
μ = 0.70
R² = 0.86
P < 0.001
(f) Leucaena
μ = 0.67
R² = 0.71
P < 0.05
(g) Thuja
μ = 0.66
R² = 0.91
P < 0.01
(h) Tomato
μ = 0.63
R² = 0.89
P < 0.001
(i) Maize
μ = 0.60
R² = 0.66
P < 0.05
(j) Acacia
μ = 0.53
R² = 0.71
P < 0.05
(k) Tobacco
μ = 0.36
R² = 0.63
P < 0.001
(l) Populus
μ = 0.31
R² = 0.76
P < 0.001
δ
PWDI_t-1

Fig. 7

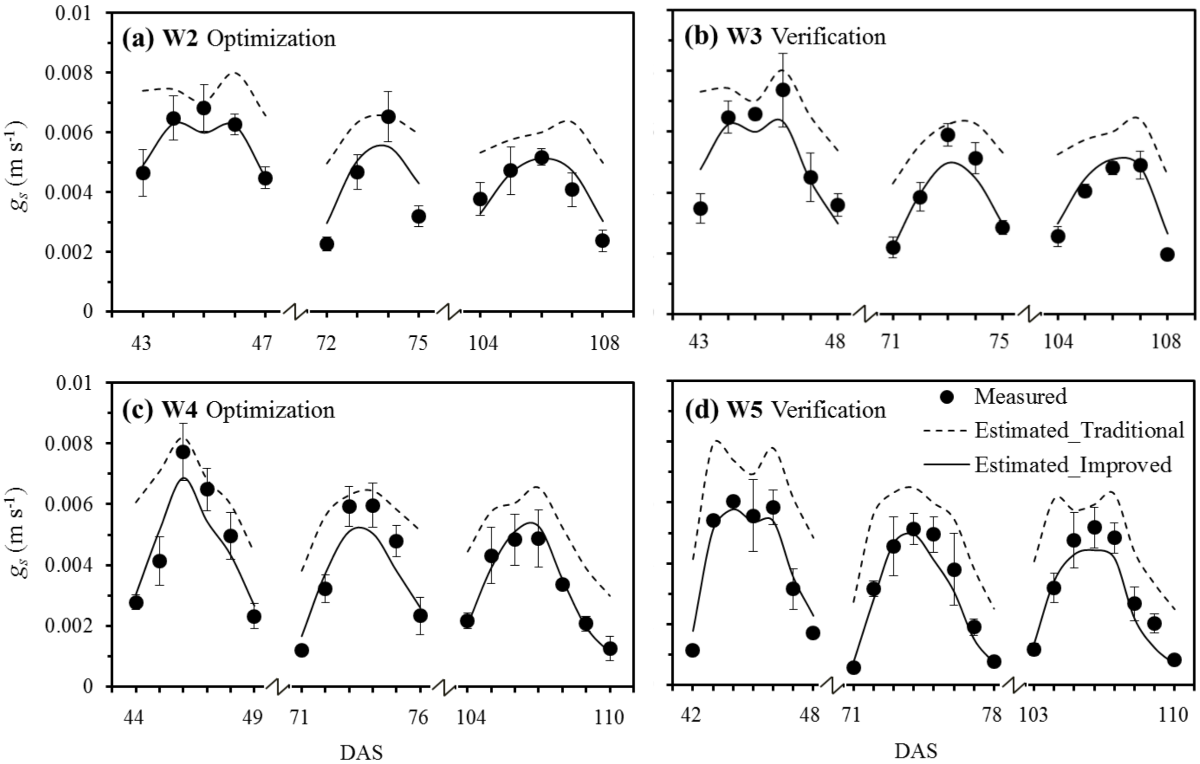
(a) W2 Optimization
(b) W3 Verification
(c) W4 Optimization
(d) W5 Verification
Measured
Estimated_Traditional
Estimated_Improved
g_s (m s^{-1})
0.01
0.008
0.006
0.004
0.002
0
43
47
72
75
104
108
48
71
44
49
76
110
42
78
103
DAS

Fig. 8

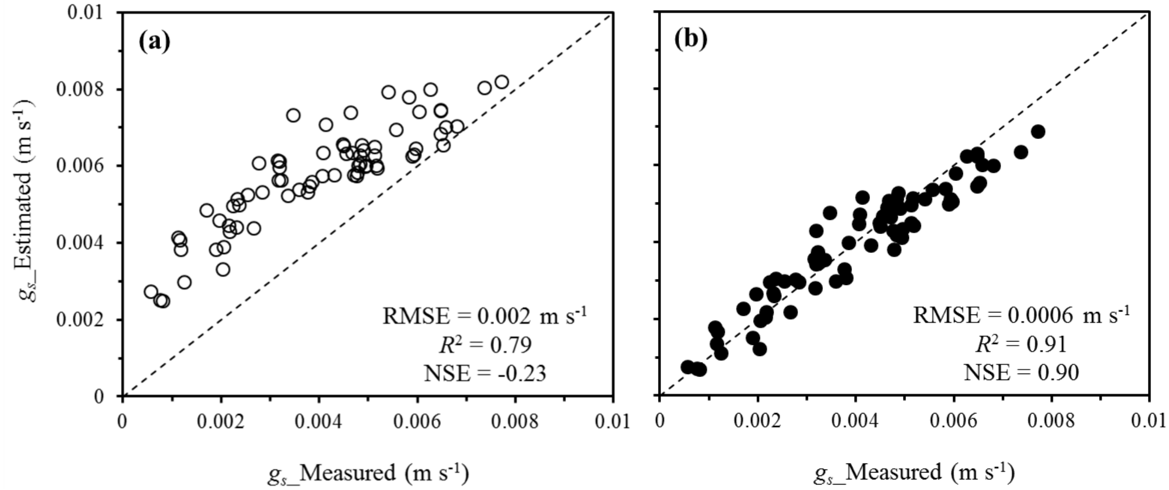
(a)
(b)
RMSE = 0.002 m s-1
R^2 = 0.79
NSE = -0.23
RMSE = 0.0006 m s-1
R^2 = 0.91
NSE = 0.90
g_s_Estimated (m s-1)
g_s_Measured (m s-1)
g_s_Measured (m s-1)
0
0.002
0.004
0.006
0.008
0.01

Fig. 9

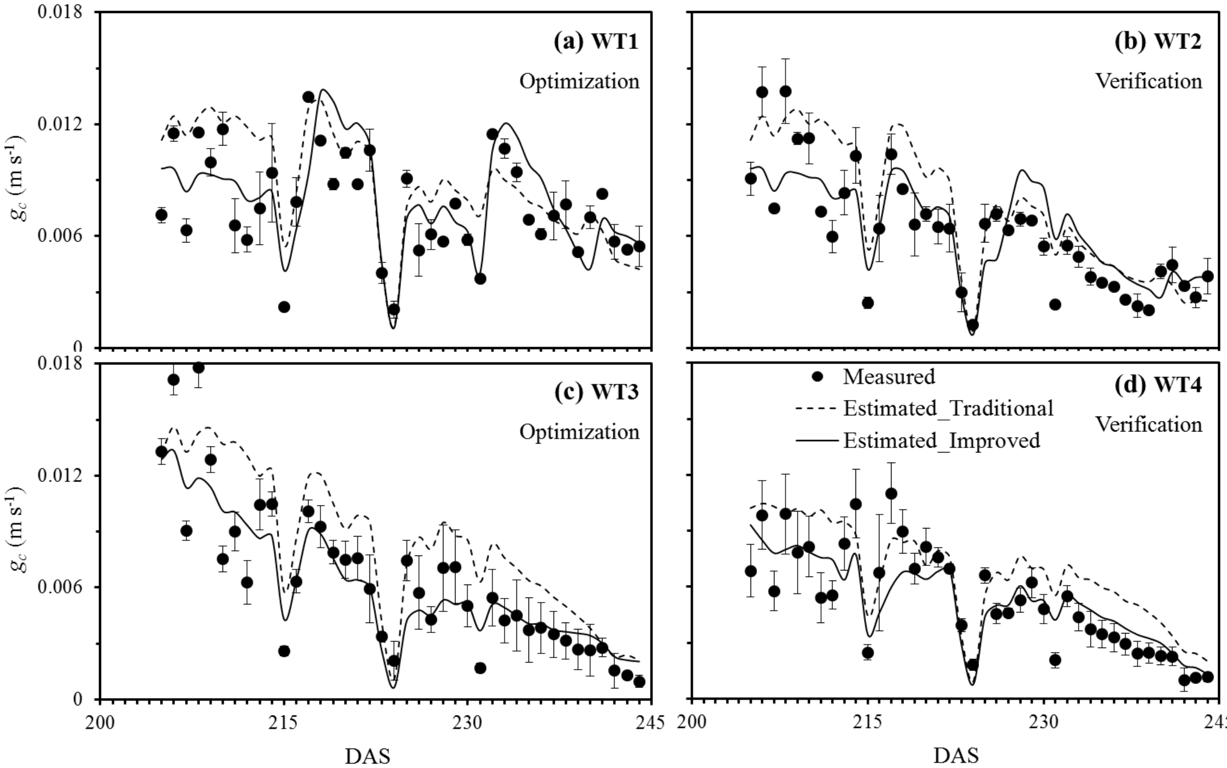
(a) WT1
Optimization
(b) WT2
Verification
(c) WT3
Optimization
(d) WT4
Verification
Measured
Estimated_Traditional
Estimated_Improved
g_c (m s-1)
0.018
0.012
0.006
0
200
215
230
245
DAS

877 **Fig. 10**

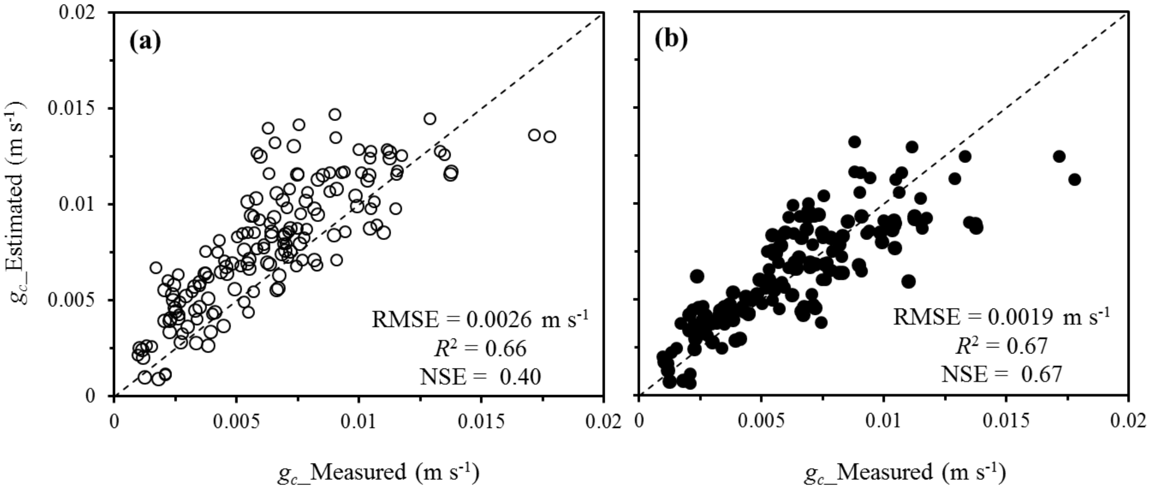

878

Fig. 11

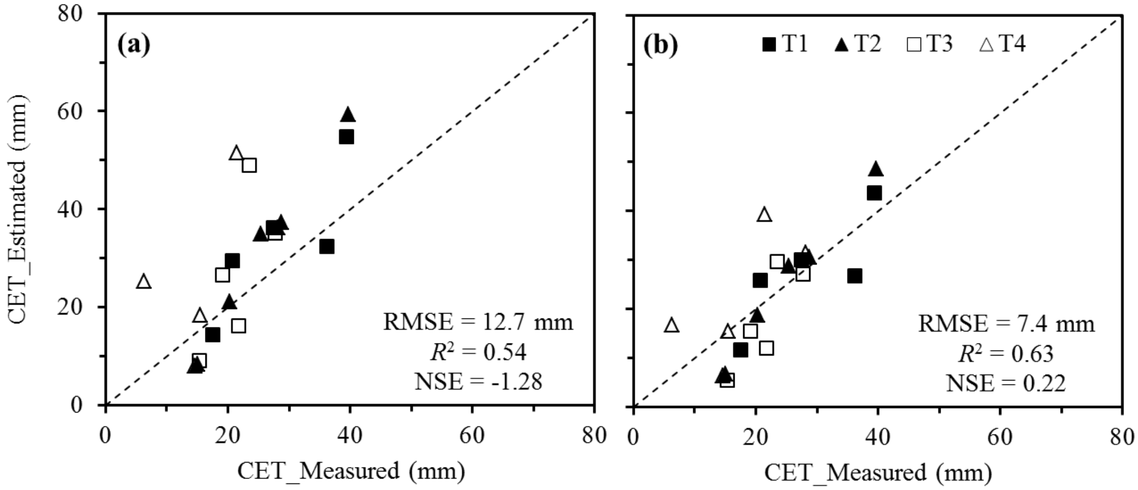
(a)
(b)
T1 T2 T3 T4
RMSE = 12.7 mm
R^2 = 0.54
NSE = -1.28
RMSE = 7.4 mm
R^2 = 0.63
NSE = 0.22
CET_Estimated (mm)
CET_Measured (mm)
CET_Measured (mm)
0
20
40
60
80

Tables

Table 1 Properties of soils used in the experiments: texture (content of sand, silt, and clay), bulk density (ρ_b), saturated water content (θ_s), field water capacity (θ_f), residual water content (θ_r), saturated hydraulic conductivity (K_s), and the fitting parameters (α and n) in van Genuchten's (1980) soil water retention curve.

Experiments	Depth	Sand	Silt	Clay	ρ_b	θ_s	θ_r	θ_f	*Ks*	α	n
	(cm)	(%)	(%)	(%)	(g cm^{-3})	(cm^3 cm^{-3})	(cm^3 cm^{-3})	(cm^3 cm^{-3})	(cm d^{-1})	(cm^{-1})	
Exp. 1	0-50	21.55	48.94	29.51	1.38	0.46	0.08	0.27	1.67	0.009	1.629
Exp. 2	0-30	49.44	45.04	5.52	1.43	0.50	0.03	0.32	5.13	0.014	1.315
	30-80	34.82	44.20	20.98	1.40	0.54	0.07	0.39	1.86	0.013	1.245
	80-230	31.92	49.90	18.18	1.56	0.55	0.06	0.41	0.12	0.020	1.177
Exp. 3	0-30	39.08	33.84	27.08	1.48	0.49	0.05	0.29	5.98	0.011	1.486
	30-70	36.10	53.28	10.62	1.49	0.53	0.04	0.20	6.27	0.017	1.675
	70-120	27.08	64.25	8.67	1.47	0.53	0.05	0.29	4.69	0.022	0.354

Table 2 Comparisons of the estimated leaf stomatal conductance g_s (Exp. 1), canopy stomatal conductance g_c (Exp. 2), and cumulative evapotranspiration CET (Exp. 3) for different treatments (independent for parameter optimization and verification) in Exps.1-3, using traditional (Eq. (10)) or improved (Eq. (11)) water stress response function for the Jarvis and/or Penman-Monteith model (RMSE, root mean squared error; R^2, determination coefficient; NSE, Nash-Sutcliffe efficiency coefficient).

Experiments	Treatments	Indicators	Models	RMSE	R^2	NSE
Exp. 1	W2, W4 (Optimization)	g_s (m s^{-1})	Traditional	0.0019	0.75	-0.26
		g_s (m s^{-1})	Improved	0.0006	0.89	0.88
	W3, W5 (Verification)	g_s (m s^{-1})	Traditional	0.0020	0.81	-0.25
		g_s (m s^{-1})	Improved	0.0005	0.92	0.91
Exp. 2	WT1, WT3 (Optimization)	g_c (m s^{-1})	Traditional	0.0028	0.61	0.32
		g_c (m s^{-1})	Improved	0.0020	0.67	0.66
	WT2, WT4 (Verification)	g_c (m s^{-1})	Traditional	0.0022	0.70	0.45
		g_c (m s^{-1})	Improved	0.0017	0.66	0.66
Exp. 3	T1, T3 (Optimization)	CET (mm)	Traditional	11.2	0.55	-1.22
		CET (mm)	Improved	6.5	0.70	0.25
	T2, T4 (Verification)	CET (mm)	Traditional	14.1	0.56	-1.48
		CET (mm)	Improved	8.2	0.67	0.15

Table 3 Water balance components under treatments T1-T4 during different growth stages of winter wheat in Exp. 3. Q, water flux across the lower boundary ("+" recharge; "-" leakage); ΔW, change of water storage ("+" increase, "-" decrease); I, irrigation; P, precipitation; CET, cumulative evapotranspiration. DAS = days after sowing.

Treatments	Indicators (mm)	Full water supplied duration	Water stressed duration				
		218-225 DAS	197-204 DAS	204-211 DAS	211-218 DAS	225-232 DAS	232-239 DAS
T1	Q	-4.4	-3.2	-3.3	-3.0	-5.0	-5.3
	ΔW	-13.8	+6.6	-5.2	+39.7	-5.8	-6.9
	$I+P$	3.3	30.8	31.0	72.9	9.9	5.3
	CET	21.6	27.4	39.5	36.2	20.7	17.6
T2	Q	-1.2	-1.7	-1.5	-1.4	-1.2	-0.8
	ΔW	-19.2	+12.3	+9.2	+28.4	-9.2	-8.9
	$I+P$	3.3	30.8	47.3	52.4	9.9	5.3
	CET	23.7	20.3	39.7	25.4	20.3	15.1
T3	Q	-1.9	-2.1	-2.1	-2.1	-1.9	-1.9
	ΔW	-14.5	+5.2	-21.3	+39.8	-10.0	-8.1
	$I+P$	3.3	30.8	0.0	56.8	9.9	5.3
	CET	19.7	27.8	23.5	19.1	21.8	15.3
T4	Q	-3.7	-3.7	-3.9	-3.3	-3.9	-3.8
	ΔW	-11.0	+6.4	-17.6	+37.6	-1.7	-5.5
	$I+P$	3.3	30.8	0.0	40.6	9.9	5.3
	CET	18.0	28.1	21.4	6.3	15.5	14.7

Table 4 Relative changes in estimating g_s (Exp. 1), g_c (Exp. 2) and CET (Exp. 3) using the Jarvis and/or Penman-Monteith model when the fitting parameters ρ and μ were fluctuated with ± 10% and ± 30% errors, respectively (g_s, leaf stomatal conductance; g_c, canopy stomatal conductance; CET, cumulative evapotranspiration).

Experiment (Estimated indicator)	Parameters	Relative change (%)			
		-30	-10	10	30
Exp. 1 (g_s)	ρ	-18.9	-5.5	4.9	13.0
	μ	6.7	2.4	-2.5	-8.1
Exp. 2 (g_c)	ρ	-19.8	-6.1	5.4	14.7
	μ	7.4	2.6	-2.7	-8.7
Exp. 3 (CET)	ρ	-13.8	-3.8	3.3	8.5
	μ	4.3	1.6	-1.7	-5.7